Reversing transgene silencing via targeted chromatin editing

Sebastian Palacios[1,2†], Elia Salibi[2†], Eric Lu [2,3], Ron Weiss [3], Thorsten M. Schlaeger[4], James J. Collins [1,3,5,6] and Domitilla Del Vecchio[2,3*]

[1] Institute for Medical Engineering and Science, Massachusetts Institute of Technology, Cambridge, MA, 02139, USA.

[2] Department of Mechanical Engineering, Massachusetts Institute of Technology, Cambridge, MA, 02139, USA.

[3] Department of Biological Engineering, Massachusetts Institute of Technology, Cambridge, MA, 02139, USA.

[4] Boston Children's Hospital Stem Cell Program, Boston Children's Hospital, Boston, MA, 02115, USA

[5] Broad Institute of MIT and Harvard, Cambridge, MA, USA

[6] Wyss Institute for Biologically Inspired Engineering, Harvard University, Boston, MA, USA

[†] These authors contributed equally to this work

[*] Corresponding author: ddv@mit.edu

Keywords: CHO-K1, human stem cells, genome engineering, epigenetics, synthetic biology

Abstract. Mammalian cell engineering offers the opportunity to uncover biological principles and develop next-generation biotechnologies. However, epigenetic silencing of transgenes hinders the control of gene expression in mammalian cells. Here, we use chromatin editing of an integrated reporter in both CHO-K1 and human induced pluripotent stem cells to dissect how histone H3 lysine 9 trimethylation (H3K9me3) and DNA methylation cooperate to maintain the silenced state and how this state can be reversed. After transient induction of either DNA methylation or H3K9me3, stable silencing was exclusively observed with both marks. Our chemical reaction model of chromatin modifications predicts that DNA methylation drives silencing maintenance. Accordingly, targeted DNA demethylation reactivated the reporter irrespective of whether silencing was achieved by inducing DNA methylation, H3K9me3, or by the endogenous cellular machinery. These results shed light on molecular mechanisms at play during silencing and provide engineering tools for potent and specific transgene reactivation in mammalian cells.

Introduction

The ability to engineer cell function is a cornerstone of biological research, engineering, and medicine[1–4]. In particular, mammalian synthetic biology offers an opportunity to study cell physiology in normal and diseased

states with unprecedented control[5], enables the manufacture of effective biotherapeutics[6,7], and supports the development of next-generation cellular therapies[8–11]. However, a major obstacle hampering the progression of such technologies from bench to bedside is epigenetic silencing of transgenes, the loss of gene expression in genomic integrations over time that is not caused by changes in the DNA sequence[12–21].

Although transgene silencing has been observed across various cell types and species, it has high relevance in CHO cells, commonly used in industrial protein production, as well as in human induced pluripotent stem cells (hiPSCs) for clinical applications. The production of therapeutic proteins in CHO cells has facilitated the diagnosis and treatment of diseases ranging from autoimmunity to cancer[22]. Despite optimizations in construct design, culture conditions and cell lines, there remains obstacles, particularly for difficult to produce antibodies[23–27]. In this case, epigenetic silencing diminishes the long-term expression profiles of genetically engineered CHO cells[28–32]. Similarly, hiPSCs derived from somatic cells have immense potential due to their ability to differentiate into any cell type. As such, these cells hold unique promise to advance the fields of human development and medicine. While human stem cells can be guided to desired cell states with chemical compounds[33–36], advances in genome engineering and synthetic biology are enabling genetic programming of hiPSCs by intrinsically controlling their differentiation to specific cell types in space and time[37–40]. However, epigenetic silencing of transgenes poses a significant efficacy and safety risk, undermining stem cell-derived therapies and delaying clinical applications. Thus, there is a need to understand the molecular mechanisms driving and maintaining silencing in order to devise strategies to mitigate it.

Epigenome engineering has emerged as a powerful tool for precise gene regulation by targeted chromatin remodeling[41–44]. The regulators comprise a DNA binding domain for specific sequence targeting and an effector domain to either directly add/remove chemical modifications to chromatin or serve as a docking site for the recruitment of endogenous factors[45–48]. The field has largely focused on the activation and silencing of endogenous genes to treat diseases associated with aberrant gene expression[49–57]. For instance, dCas9 fused to DNMT3A/L and KRAB domains was used to downregulate *pcsk9* gene expression with the aim of decreasing circulating low-density lipoprotein cholesterol levels *in vivo*[58]. By fusing DNMT3L cofactor to a DNA binding domain and a histone 3 tail, it was possible to recruit and activate endogenous DNMT3A in cells to methylate and repress a locus involved in prion protein production[59]. Another study recruited dCas9-TET1 fusion protein to specifically demethylate the *brca1* tumor suppressor gene implicated in breast cancer[60]. Moreover, epigenome editing was used to rescue diseased phenotypes in neurons derived from Rett Syndrome and Fragile X Syndrome patients by TET1-mediated DNA demethylation at *mecp2* and *fmr1* loci, respectively[61,62]. DNA demethylating systems have further been used to reverse the silencing of the imprinted locus involved in Prader-Willi syndrome[63].

In contrast to epigenetic editing of endogenous genes, epigenetic editing of transgene loci remains under-explored, especially in hiPSCs. Two prior studies demonstrated rescue of a doxycycline-inducible system in mouse embryonic stem cells and transgenic mice by fusing TET1 catalytic domain to the rTetR-transactivator (rtTA)[64,65]. A different study explored silencing dynamics following epigenetic editing with different chromatin regulators by recruiting them to a reporter system on a human artificial chromosome in CHO-K1 cells[46]. Similarly, a study in CHO-K1 cells used chromatin regulators to show that gradients of DNA methylation are stable and correlate with gene expression[66]. The CRISPRoff/on system was developed by fusing different epigenetic activators or repressors to dCas9 and was validated on a reporter transgene introduced into HEK293T cells via lentiviral transduction[45]. A study demonstrated the synergy of recruiting combinations of epigenetic regulators (KRAB/DNMT3A/L) to a synthetic reporter locus in multiple cell types[49]. Another work in CHO cells built a synthetic promoter library with varying CpG content and proceeded to epigenetically repress it to reveal a relationship between silencing rate and CpG content[67]. Lastly, different DNMT3A/L variants were characterized for their methyltransferase and gene silencing activities in HEK293 and Jurkat T cells with lentiviral insertion of the reporter transgene[68]. Although these works provide significant advancements, they are performed in different cellular and genomic contexts making it difficult to paint a unified picture of silencing and reactivation dynamics. Moreover, to the best of our knowledge, there is no demonstration of transgene reactivation in human induced pluripotent stem cells. This highlights the need to investigate transgene silencing and reactivation in a more controlled cellular and genetic setting, using chromosomal site-specific integration of a reporter system, in both differentiated cells and pluripotent stem cells.

Here, we explore the potential of engineered chromatin regulators to silence and reactivate transgenes in mammalian cells, particularly in hiPSCs, as a basis for the transcriptional control of genetic circuits by chromatin modifications. We first demonstrate the activity of our engineered chromatin regulators at a synthetic chromosomal reporter locus in CHO-K1 cells. We then move to investigate silencing and reactivation of the same synthetic reporter system but integrated in hiPSCs. We test the ability of these chromatin regulators to reactivate reporter gene expression both after epigenetic silencing by chromatin editing and after endogenous silencing. Our chromatin state data educate a model of chromatin modifications that allows us to disentangle the molecular mechanisms at play during epigenetic editing and predicts the silencing and reactivation dynamics observed in our experiments.

Results

Switching transcriptional state by targeted chromatin editing in somatic mammalian cells

We first set out to investigate whether we could control epigenetic and transcriptional states in chromosomal integrations via chromatin editing. To this end, we utilized an experimental system that we previously developed in CHO-K1 cells (Fig. 1A), a primary model cell line for synthetic biology with wide use in biotechnology[66]. This system comprises a single-copy, site-specific integration of a reporter cassette in the Rosa26 locus. The reporter cassette includes a fluorescent protein (EBFP2) driven by a constitutive promoter (hEF1a) with upstream operator sites that allow recruitment of DNA binding domains fused to chromatin regulators (Fig. S1A), thus enabling targeted editing of chromatin at the locus (See Methods). To assess our ability to control chromatin states, we subjected cells in the active state to transient transfection with DNMT3A, a *de novo* DNA methylation writer[69], fused to rTetR for sequence-specific targeting (rTetR-DNMT3A). We then transiently transfected silenced cells with rTeTR-TET1, comprising the TET1 catalytic domain[57] fused to rTetR (or TetR when specified) for sequence-specific targeting (see Methods and Supplementary Table 1). Reporter gene expression was monitored by time-resolved flow cytometry (Fig. 1B).

We co-transfected rTetR-DNMT3A along with EYFP, which we use as a proxy for rTetR-DNMT3A expression levels[70,71], isolated transfected CHO-K1 cells (EYFP+) by fluorescence-activated cell sorting (FACS) two days later and monitored fluorescence changes by flow cytometry. We observed a steady decrease in reporter gene expression over the course of 8 days, reaching complete silencing by day 10 (Fig. 1C, S1B). Gene expression levels remained low after withdrawal of doxycycline (dox), indicating that the reporter was stably silenced. After 20 days, we co-transfected the silenced cells with rTetR-TET1 and EYFP transfection marker, isolated transfected cells (EYFP+) by FACS and continued monitoring fluorescence. Already 4 days post rTetR-TET1 transfection, the reporter was fully reactivated and remained active after dox withdrawal, indicating stable reactivation. We additionally compared reactivation strength of different transfection levels of rTetR-TET1 by FACS, noting that medium to high levels displayed the best performance in terms of trade-off between reactivation strength and leakiness (Fig. S1C-D). While DNMT3A recruitment durably silenced transgene expression, transient transfections with KRAB domain, a regulator known to indirectly recruit histone 3 lysine 9 trimethylation (H3K9me3)[72], led to transient repression in CHO-K1 cells (Fig. S1E and[66]). We observed no silencing when transfecting the KRAB or DNMT3A domains without targeting (Fig. S2A), and little to no reactivation when transfecting TET1 or

rTetR alone (Fig. S2B). These results demonstrate the ability of our system to be toggled between active and silenced states efficiently following transient transfection of the engineered chromatin regulators.

We further characterized the chromatin marks at the reporter locus 10 days after transfection with the chromatin regulators. We performed quantitative PCR (qPCR) following methylated DNA immunoprecipitation (MeDIP-qPCR) to assess DNA methylation levels and Cleavage Under Targets and Release Using Nuclease (CUT&RUN-qPCR) to assess H3K9me3 levels (see Methods). The data show that DNMT3A recruitment results in enrichment for DNA methylation as expected with a 15-fold increase compared to active cells (Fig. 1D, left). We also detected a fold increase of H3K9me3 although to a lesser degree, suggesting that DNA methylation recruits writers of H3K9me3, which is consistent with prior reports[46]. After targeted chromatin editing with rTetR-TET1, both DNA methylation and H3K9me3 marks were reduced to approximately 10% and 25% of that in silenced cells, respectively (Fig. 1D, right), suggesting that H3K9me3 cannot sustain itself in the absence of DNA methylation.

In addition to employing the TET1 catalytic domain, we attempted to reactivate the silenced transgene with other relevant chromatin regulators (Fig. 1E, S2C). In particular, we employed catalytic domains of DOT1L, a histone 3 lysine 79 methyltransferase (H3K79me2), the p300 core domain, a histone 3 lysine 27 acetyltransferase (H3K27ac), and PRDM9, a histone 3 lysine 4 methyltransferase (H3K4me3), and their combinations since H3K79 and H3K4 methylation were described to act synergistically[48,54,73]. No reporter gene expression could be detected by flow cytometry for those conditions that excluded the TET1 domain, suggesting that recruitment of activating histone modifications is alone insufficient to allow expression from a transgene loaded with DNA methylation. To test whether transcriptional activator domains would promote gene expression, we utilized the VP64-p65-Rta (VPR) transcriptional activator[74] fused to dCas9 with a guide RNA (gRNA) targeting all the TetO sites (Fig. 1F, S2D). VPR recruitment resulted in a burst of gene expression soon after transfection but slowly returned to basal levels over the course of 8 days. In contrast, TET1 recruitment resulted in a steady increase in gene expression that remained stable for the duration of the experiment, again highlighting the need to demethylate the locus for durable reactivation. We could recapitulate the results when swapping the hEF1a promoter with other frequently used constitutive promoters (CAG, PGK and UbC, see Supplementary Table 2), showing responsiveness to both silencing by rTetR-DNMT3A and reactivation by rTetR-TET1 (Fig. S3).

Targeted chromatin editing can stably silence the reporter system in hiPSCs

We extended our investigation to determine whether we could also efficiently program the epigenetic state of a transgene in hiPSCs. To this end, we sought to construct the reporter gene in human stem cells utilizing

landing pad technology for site specific recombinase mediated integration[75,76], which could closely recapitulate the chromosomal integration of the reporter gene we developed in CHO-K1 cells. We consequently developed an hiPSC landing pad cell line and performed chromosomal integration of the reporter system in human stem cells (Fig. 2A, S4A and Methods). The chromosomal integration lies in the AAVS1 locus, a genomic region that is widely utilized for transgene integration in human cells[77]. Despite its widespread adoption, there are mixed reports of transgene expression stability in the AAVS1 locus in human stem cells[78–82], hinting at a context-dependent behavior, potentially stemming from the insulator-promoter-gene triad employed.

We set out to study different modalities of epigenetic silencing in human stem cells. Specifically, we aimed to silence gene expression via *de novo* DNA methylation or via recruitment of H3K9me3 writers using our engineered chromatin regulators (see Methods), rTetR-DNMT3A and PhlF-KRAB, respectively (Fig. 2B-C). To investigate silencing via *de novo* DNA methylation, we co-transfected rTetR-DNMT3A and EYFP transfection marker, isolated transfected stem cells (EYFP+) by FACS and performed flow cytometry measurements on day 2 just after sorting and on day 12 (Fig. 2B). The cells cultured with dox for 8 days exhibited efficient silencing at day 12, long after dox was omitted and the EYFP transfection marker was diluted indicating absence of rTetR-DNMT3A in the system (Fig. 2D). Thus, by transiently recruiting solely DNMT3A and depositing DNA methylation *de novo*, we achieved silencing that persisted even after withdrawal of the regulator. Next, we attempted to silence the cells via H3K9me3 deposition. We transfected the cells with PhlF-KRAB and EYFP, isolated transfected (EYFP+) stem cells using FACS and subsequently performed flow cytometry measurements at day 2, after sorting, and again at days 10 and 12 (Fig. 2C). The cells cultured in the absence of DAPG silenced efficiently and remained silenced after transient KRAB-mediated chromatin editing (Fig. 2E), suggesting stable silencing similar to that achieved with DNMT3A treatment.

Chromatin analysis of DNA methylation and H3K9me3 revealed that addition of one chromatin mark led to recruitment of the other in both cases (Fig. 2F). In summary, when transiently recruiting either DNMT3A or KRAB domain to the transgene locus in hiPSCs, we observed stable silencing and an increase in both DNA methylation and H3K9me3 marks, independently of the fusion protein employed for repression. These data indicate that DNA methylation mediates the recruitment of writers of H3K9me3 as in CHO-K1 cells (Fig 1D)[46,66], and also suggest that H3K9me3 mediates the recruitment of DNA methylation writers in hiPSCs, different from what was reported in CHO-K1 cells where H3K9me3 deposition does not lead to enrichment of DNA methylation and hence results in transient repression (Fig. S1E)[66]. Intriguingly, when we repeated the silencing experiments with a CAG promoter-driven reporter (we excluded UbC and PGK promoters here due to low fluorescence signals from reporter lines), DNMT3A alone had no effect on gene expression while KRAB resulted only in a transient repression (Fig. S4B). However, co-transfection of both chromatin regulators led to sustained repression until 19

days post-transfection, suggesting again a synergy between DNA methylation and H3K9me3, and indicating that this synergy may depend on the specific promoter.

A chromatin modification model predicts silencing and reactivation dynamics in hiPSCs

To shed light on the molecular mechanisms at play during silencing, we developed a chemical reaction model of DNA methylation and H3K9me3, largely based on a previously published model[83] but educated by our chromatin analysis data (Fig. 2F). After targeted chromatin editing with DNMT3A, we observed not only DNA methylation as expected, but also H3K9me3 (Fig. 2F, left), consistent with prior reports that methylated CpGs bind to proteins (such as Methyl-CpG-binding Protein 2, MECP2) that recruit H3K9me3[84]. The model thus includes the recruitment of H3K9me3 by DNA methylation, leading to a chemical reaction path from unmodified nucleosomes (U) to nucleosomes with DNA methylation only, denoted by (y), to nucleosomes with both marks, denoted by (z) (Fig. 3A). Similarly, targeted chromatin editing with KRAB led to H3K9me3 deposition as expected, but also to DNA methylation (Fig. 2F, right), consistent with prior reports indicating that H3K9me3 can be bound by proteins that recruit DNMT3A[85,86]. Accordingly, the model accounts for the recruitment of DNA methylation by H3K9me3, leading to a chemical reaction path from unmodified nucleosomes (U) to nucleosomes with H3K9me3 only, denoted by (x), to nucleosomes (z) with both marks (Fig. 3A). Positive feedback thus emerges around the state z because DNA methylation and H3K9me3 recruit each other (arrows marked by β and β_0). Moreover, H3K9me3 is autocatalytic as it recruits its own writers, what is known as heterochromatin spreading[87–89] (feedback loop marked by α in Fig. 3A). Finally, H3K9me3 decays passively through dilution and actively by the action of histone demethylases (green arrows in Fig. 3A, marked by δ). In contrast, DNA methylation is stable due to the maintenance action of DNMT1 when TET1 eraser enzyme is absent[90,91]. Therefore, the decay rate of DNA methylation is negligible when no TET1 is recruited but increases proportionally with the amount of TET1 present (blue arrows in Fig. 3A). The full set of reactions is reported in Supplementary Text.

Recapitulating silencing dynamics in hiPSCs. According to the model, starting from an active gene state that lacks DNA methylation and H3K9me3, transient and efficient recruitment of DNMT3A will lead to the permanent establishment of DNA methylation, which will, in turn, lead to the permanent establishment of H3K9me3, and *vice versa* (Fig. 3B-C, before time T). Consequently, we should observe permanent silencing in both cases, which is consistent with the experimental data pertaining to the hEF1a promoter (Fig. 2D-E). Nevertheless, the model suggests that the extent of silencing depends on the fraction of established DNA methylation at the locus, which is directly proportional to the strength of positive feedback (α, β, and β_0) and the rate of *de novo* DNA methylation by DNMT3A. If the rate of *de novo* DNA methylation is exceedingly low such that it is mostly established through the

recruitment by H3K9me3, then it is possible that DNA methylation can only be established when both KRAB and DNMT3A are concurrently recruited to the promoter, but not with DNMT3A alone (Fig. S5, middle and bottom plots). Similarly, the effective recruitment of DNA methylation by H3K9me3 hinges on a sufficiently large rate constant β, which increases with the local availability of free DNMT3A and H3K9me3-binding proteins that recruit DNMT3A. For low values of the rate constant, H3K9me3 alone will not recruit sufficient DNMT3A to stabilize the silenced state, resulting in decay of H3K9me3 and transient silencing (Fig. S5, top plot). However, exogenous delivery of DNMT3A (via transient transfection) in the presence of H3K9me3 can increase this rate and enable the establishment of DNA methylation, leading to durable silencing of the locus, also in agreement with our experimental data pertaining to the CAG promoter driving reporter expression (Fig. S4B).

Predicting reactivation dynamics in hiPSCs. In the presence of high levels of TET1, the chromatin modification circuit of Fig. 3A will be devoid of DNA methylation (DNAme), such that the system reduces to the two-state circuit of Fig. 3D. In this circuit, unmodified nucleosomes (U) become modified to H3K9me3 (x) through positive feedback (α), and modified nucleosomes become unmodified through decay (δ). The steady state values of the fraction of H3K9me3 (x) are obtained when the production and decay terms are equal: $\alpha \cdot x \cdot (1-x) = \delta \cdot x$ (Fig. 3E, and Supplementary Text). When $\alpha \gg \delta$, that is, the autocatalysis overpowers decay, two steady states appear, but only the non-zero one corresponding to maximum H3K9me3 located at $x = (\alpha - \delta)/\alpha \approx 1$ is stable (the silenced state). Conversely, when $\alpha \ll \delta$, meaning decay overpowers autocatalysis, the system has only one stable steady state at $x \approx 0$ completely lacking H3K9me3 (the active state). Therefore, only in the latter case can we expect gene reactivation after TET1 recruitment since removal of DNA methylation will also lead to H3K9me3 decay. Prior data in CHO-K1 cells revealed that H3K9me3 could not sustain itself in the absence of DNA methylation (S1E)[66], suggesting that H3K9me3 decay overpowers autocatalysis in these cells ($\alpha \ll \delta$). If this holds in hiPSCs as the CAG promoter data suggest (Fig. S4B), we should expect that the state should stay at $x \approx 0$ and the system should remain devoid of both DNA methylation and H3K9me3 even after removal of TET1, exhibiting durable gene reactivation (Fig. 3B-C, after time T and $\alpha \ll \delta$). In contrast, if autocatalysis overpowers decay ($\alpha \gg \delta$), transient recruitment of TET1 will not lead to the decay of H3K9me3 by DNA methylation erasure, and hence gene expression would remain silenced (Fig. 3B-C, after time T and $\alpha \gg \delta$).

The approximated model of Fig. 3D assumes that TET1 completely erases DNA methylation when recruited. However, in practice, residual amounts of DNA methylation can remain. In the complete model of Fig. 3A, this residual level will reinforce H3K9me3 (through β_0), which will reciprocally reinforce DNA methylation (through β). If this positive feedback loop is sufficiently strong, the system can restore DNA methylation and H3K9me3 levels after removal of TET1 thereby silencing the locus again. In this case, TET1 alone would lead to transient reactivation, possibly requiring a combination of TET1 and H3K9me3 erasers to achieve durable reactivation. It

follows that for both marks to be permanently erased after transient recruitment of TET1, it is also necessary that the positive feedback loop between DNA methylation and H3K9me3 is sufficiently weak relative to the decay of H3K9me3 (Fig. S6).

Reversing targeted epigenetic silencing in hiPSCs

The reactivation of the silenced transgene in CHO-K1 cells using rTeTR-TET1 along with the model predictions suggested that similar reactivation could occur in hiPSCs if the positive feedback between DNA methylation and H3K9me3, as well as H3K9me3 autocatalysis, are sufficiently weak. We therefore attempted reactivating the reporter system using rTetR-TET1 in hiPSCs previously silenced with DNMT3A or KRAB. To probe reactivation dynamics, we co-transfected cells with rTetR-TET1 and EYFP transfection marker, isolated transfected cells (EYFP+) at day 2 by FACS and periodically measured reporter gene expression by flow cytometry (Fig. 4A). As predicted by the model, DNMT3A-silenced iPSCs transfected with rTetR-TET1 and cultured in dox for 6 days displayed strong reactivation of gene expression 7 days post-transfection, which remained stable for the duration of the experiment (Fig. 4B). Transfection marker (EYFP) levels indicate that the chromatin regulator was completely diluted out by day 7, implying that expression levels were stable in the absence of the regulator. Interestingly, when we repeated the experiment using KRAB-silenced hiPSCs, we similarly observed efficient and stable reactivation of transgene expression up to 15 days post-transfection (Fig. 4C). Chromatin analysis of DNA methylation and H3K9me3 revealed that both marks were depleted after rTetR-TET1 recruitment in both cases (Fig. 4D), in line with model predictions (Fig. 3B-C). The data corroborate the model predictions that H3K9me3 autocatalysis and the positive feedback between H3K9me3 and DNA methylation are overpowered by H3K9me3 decay. This suggests that it is possible to reactivate silenced loci even when there are repressive histone marks without necessitating direct H3K9me3 erasure.

To confirm that pluripotency was unaffected by epigenome editing with TET1 overexpression, we performed live cell microscopy to assess colony morphology and transgene expression in addition to quantification of pluripotent surface marker expression (TRA-1-60)[92] by flow cytometry (Fig. 4E-H). Cells reactivated following DNMT3A-silencing displayed colonies with smooth edges and high EBFP2 fluorescence (Fig. 4E and S7A) while maintaining >90% of the population expressing the TRA-1-60 pluripotency marker (Fig. 4F). Similarly, KRAB-silenced iPSCs reactivated with TET1 formed colonies with smooth edges and devoid of spontaneously differentiated cells while expressing EBFP2 (Fig. 4G and S7B), and the vast majority of the population stained positive for the TRA-1-60 surface marker (Fig. 4H). Unlike dCas9-VPR, transient recruitment of TetR-TET1 to the silenced CAG-driven reporter also reactivated gene expression, suggesting that the reactivation function of TET1

generalizes across promoters (Fig. S7C). Together, these results indicate that our targeted chromatin editing does not negatively impact stem cells while still managing to transcriptionally modulate the transgene locus for durable silencing or reactivation in hiPSCs.

Reversing endogenous silencing in hiPSCs

Motivated by the result that transgene reactivation was possible from both silenced states, we asked whether we could reverse endogenous epigenetic transgene silencing. To this end, we first isolated hiPSCs in the active state (EBFP2+) by FACS and cultured them under standard conditions for 12 days, anticipating the emergence of an endogenously-silenced population (EBFP2-) that we subsequently isolated by FACS (Fig. 5A, bottom panel red gate). We then repeated the experiment outlined in Fig. 4A but starting with the EBFP2- sorted population. The cells transfected with rTetR-TET1 (EYFP+) and cultured in dox for 6 days showed efficient reporter gene reactivation at day 7 that persisted until day 15 (Fig. 5B). A small increase in the fraction of silenced cells is noticeable between days 7 and 15, which is likely due to endogenous silencing since they are lacking rTetR-TET1 based on EYFP expression. Chromatin analyses of the promoter region revealed that rTetR-TET1 recruitment (dox+) led to a significant decrease in the levels of both DNA methylation and H3K9me3 when compared to the silenced cells (Fig. 5C). We also tested other activator domains to compare their ability to reactivate gene expression in hiPSCs (Fig. 5D). For the rTetR-P300 fusion protein, we could not detect reporter expression after 2 or 8 days post transfection, indicating that recruitment of a histone acetylase is not conducive to reactivation at a methylated locus. Next, the combination of rTetR-PRDM9 and rTetR-DOT1L initially displayed slight EBFP2 fluroescence at day 2, but the activation was not stable and decreased to the initial silenced level by day 8. We observed similar behavior when targeting dCas9-VPR to all TetO sites, with an initial burst in fluorescence that faded with time. In fact, the only durable activation we observed was when transfecting rTetR-TET1. These cells displayed a smaller increase in fluorescence at day 2 when compared to DOT1L/PRDM9 or VPR targeting, but showed strong fluorescence signal at day 8. These data demonstrate that transgene loci endogenously silenced by DNA methylation and H3K9me3 can be stably reactivated by removing DNA methylation only, which then leads to an automatic loss of the H3K9me3 mark. Reactivated cells maintained their pluripotency, as is shown by microscopy analysis of colony morphology (Fig. 5E and S8A) and expression of cell surface marker TRA-1-60 (Fig. 5F).

We further corroborated the data by performing bulk RNAseq on active cells as well as endogenously silenced cells before and after reactivation with TET1 to confirm specific targeting and exclude any off-target effects (Fig. 5G and S8B-C). The data clearly show downregulation of EBFP2 between active and silenced cells and

subsequent upregulation between silenced and reactivated (TET1) cells. Importantly, when comparing active cells to reactivated cells (Fig. S8C), we found no difference in gene expression profiles between the two samples, indicating that reactivation did not result in undesired transcriptional changes and that the reactivated cells returned to their original state before endogenous silencing. We did observed a slight non-specific transcriptional up-regulation of a few endogenous genes between silenced and reactivated (TET1) cells. In particular, ZFP42 or REX1 (on chromosome 4q35), RBM46 (on chromosome 4q32), and LEFTY1 (on chromosome 1q42) were upregulated in reactivated cells relative to silenced cells. The ZFP42 transcription factor showing highest expression fold change is broadly associated with pluripotency maintenance, consistent with a transient activation of pluripotency genes[93], while LEFTY1, a secreted inhibitor of SMAD signalling[94], borders the expression fold change limit and is associated with early developmental gene modules. RBM46 instead displays an intermediate expression fold change with respect to the other two genes, and is a testis- and germline-enriched RNA-binding protein localizing to the cytoplasm[95]. Despite these differences, it is noteworthy that the relative endogenous gene expression changes between silenced and reactivated cells are thwarted by the significant transcriptional modulation elicited on the targeted EBFP2 reporter transgene. Overall, the results suggest that the our system for TET1-mediated transgene reactivation is highly specific to the targeted locus and leads to little off-target effects while restoring transgene expression to its original levels.

Discussion

While epigenome engineering has made great strides in understanding chromatin dynamics and the interplay between chromatin marks, a systematic investigation within a controlled genetic context of the molecular mechanisms at play in transgene silencing and reactivation had been lacking. Here, we developed a reporter system in two different cell types that differ in the locus of integration, but are otherwise identical, to investigate transcriptional control by chromatin editing (Fig. 1A-B, 2A-C, 4A). We demonstrated that transient expression of rTetR-DNMT3A can durably silence the transgene in both cell types and that it leads to an increase in both DNA methylation and H3K9me3 at the promoter region (Fig. 1C-D, 2D-F). The mathematical model we developed (Fig. 3A) predicted the ability to reactivate gene expression by targeted DNA demethylation despite having repressive histone marks (H3K9me3) at the locus if the rate of H3K9me3 autocatalysis is sufficiently lower than its turnover (Fig. 3B-C; top panels). In this case, locus repression is maintained by DNA methylation and can only be relieved by erasing it, leading to a steady decrease in H3K9me3 and a concomitant increase in gene expression. The experiments with transient expression of rTetR-TET1 in silenced cells further demonstrated that we can rescue transgene expression from any constitutive silenced state and that both DNA methylation an H3K9me3

are diminished (Fig. 1C-D, 4B-D, 5B-C), which, to the best of our knowledge, had not been demonstrated at site-specific genomic integrations in hiPSCs.

We observed that the reporter system in CHO-K1 cells transiently transfected with PhlF-KRAB display only transient silencing with expression levels returning to normal after PhlF-KRAB dilution (Fig. S1E and[66]), concordant with other reports using CHO-K1 cells and the KRAB domain[46]. Transient recruitment of dCas9-KRAB was also reported to lead to transient repression of a reporter system in HEK293T cells, requiring the co-recruitment of DNMT3A/L to exhibit stable silencing[45]. These observations suggest that while H3K9me3 recruitment by KRAB reversibly represses gene expression, stable silencing may be achieved by combining DNA methylation in these genomic contexts. Contrarily, when we repeated the KRAB-silencing experiment in hiPSCs, we observed stable silencing (Fig. 2E). This discordant behavior between CHO-K1 and hiPS cells might be attributed to differing epigenetic regulatory networks governing DNA methylation and H3K9me3. Specifically, H3K9me3 leads to the recruitment of DNA methylation in hiPSCs (Fig. 2F) but not in CHO-K1 cells[46,66], indicating that the permanence of H3K9me3 in hiPSCs may be due to the positive feedback between DNA methylation and H3K9me3 (Fig. 3A), which is instead lacking in CHO-K1 cells[66].

This context-dependence of the network of chromatin modifications can be attributed to the presence of molecular players enabling the interactions, which in turn may be conditioned to the specific cell type, genomic integration site, and promoter. For instance, the protein UHRF1, consisting of Tandem-Tudor domain (TTD), plant homeodomain (PHD) and SET and RING associated domain (SRA), can bind H3K9me2/3, H3K4me0/1 and hemimethylated DNA in addition to recruiting maintenance methylase DNMT1 and *de novo* methylases DNMT3A/B[96–100]. While this protein has been observed experimentally in humans (*Homo sapiens*), it is only predicted to be present in hamsters (*Cricetulus griseus*) (see UniProt entries Q96T88 and A0A8C2LY95, respectively), which might explain why H3K9me3 leads to DNA methylation in hiPSCs but not in CHO-K1 cells. However, a study has shown reversibility of KRAB-induced silencing of CAG driven reporter in human iPSCs but stable silencing in hiPSC-derived cardiomyocytes[101], similar to what we observed with CAG reporter silencing with KRAB (Fig/ S7C), suggesting that these parameters may depend on the promoter and cell differentiation state rather than on the species identity alone.

The network of interactions among chromatin marks may also depend on the specific promoter used, although our data indicate that a variety of commonly used mammalian promoters, including CAG, murine PGK, and human UbC promoters, can be similarly silenced and re-activated in CHO-K1 cells (Fig. S3). In contrast, we found that the silencing and reactivation dynamics of the CAG promoter was different from that of the hEF1a promoter in hiPSCs (Fig. 2D-E, S4B and S7C). Specifically, KRAB-based chromatin editing of CAG-driven expression led

to transient silencing, as in CHO-K1 cells and other reports[101], while DNMT3A-based editing did not exert any effect. However, combining both chromatin regulators resulted in durable silencing (Fig. S4B), which could be reversed by TET1-mediated reactivation (Fig. S7C), similarly to what we observed for the hEF1a promoter in hiPSCs and CHO-K1 cells. The model recapitulates these differences when DNA methylation recruitment by H3K9me3 is contingent on the recruitment of rTetR-DNMT3A to the promoter (Fig. S5). In fact, the strength of this recruitment (β) is proportional to the availability of both free DNMT3A at the promoter and H3K9me3-binding proteins that also bind to DNMT3A. If there is an abundance of the latter but not of the former, recruitment of H3K9me3 alone is insufficient to recruit endogenous DNMT3A, which results in transient repression after KRAB editing. When we express rTetR-DNMT3A and H3K9me3 is present, this can recruit DNMT3A more effectively to the promoter to establish stable DNA methylation and consequently, lead to durable repression. In the absence of H3K9me, rTetR-DNMT3A recruitment to the locus is insufficient to establish stable DNA methylation patterns, thus having no effect on the transcriptional state of the reporter gene.

Prior work investigated the reactivation of endogenous genes that were either hypermethylated or unmethylated with PRDM9 or VP64, concluding that reactivation cannot be sustained for an extended period of time without first removing DNA methylation at the locus, which they showed with a nucleoside analog[73]. Our data corroborates this conclusion for transgenes, since we were unable to durably reactivate the silenced reporter with the other chromatin regulators or transcriptional activators tested in either CHO-K1 (Fig. 1E-F) or hiPSCs (Fig. 5D). Other studies have shown gene reactivation by targeted DNA demethylation in both endogenous and integrated genes in a variety of cell lines, suggesting that reactivation was possible for genes silenced by DNA methylation[45,50,57,64,102]. However, it was unknown whether TET1 recruitment to a KRAB-silenced locus would also lead to gene reactivation. Our results clearly show it is possible (Fig. 4E-F), and indeed, we reliably reactivated the endogenously silenced reporter with hEF1a or CAG promoter in hiPSCs by targeting TET1 catalytic domain (Fig. 5C and S7C), showing removal of repressive chromatin marks at the hEF1a promoter (Fig. 5D). Different from previous studies, TET1 delivery was transient but lead to durable reactivation (see Fig. 5B-C, EYFP marker at day 15). We did observe a small increase in the fraction of silenced cells between days 7 and 15, indicating that while the reporter was reactivated, it nonetheless remained susceptible to endogenous silencing. These results are particularly relevant for engineering cell fates since transgenes have been implicated as targets for the human silencing hub (HUSH) complex that ultimately leads to H3K9me3 and subsequent DNA methylation deposition[17,19,103,104]. We thus have demonstrated how to achieve potent and selective gene reactivation in hiPSCs, paving the way for maintenance of expression in genetic circuits susceptible to silencing by endogenous cellular machinery.

Limitations of the Study. The system developed here has its limitations, firstly due to context-dependent

responses of different loci after the same treatment for it was shown that at certain genomic loci, H3K9me3 and DNA methylation are insufficient for durable gene repression[105–107], whereas in other reports stable silencing can only be achieved by both H3K9me3 and DNA methylation[108]. Nonetheless, we have seen that the AAVS1 locus is stably repressed by these marks in hiPSCs when gene expression is driven by the hEF1a promoter, which we are able to rescue by rTetR-TET1 recruitment. We have summarized the divergent findings in a schematic that depicts the silencing and reactivation of an AAVS1 transgene locus in Fig. 6. Context-dependencies may also arise from using a different promoter-operator pair than the 5xPhlO-5xTetO-hEF1a combination, especially if the promoter differs in strength or CpG content[67], whereas different DNA-protein binding pairs (for instance the Gal4-UAS system) might offer different levels of repression and activation. Further limitations are that the cells need to be amenable to transfection, and that the delivery of the chromatin regulators that provide a determinate reactivation is only transient, making it unsuitable for long-term applications where cells might re-silence. However, both limitations can be resolved by chromosomally integrating the rTetR-TET1 expression cassette along with the promoter-operator system. We envision this anti-silencing genetic module to be useful for genetic engineering and to enable the development of cellular therapies with increased circuit complexity.

Main figures and captions

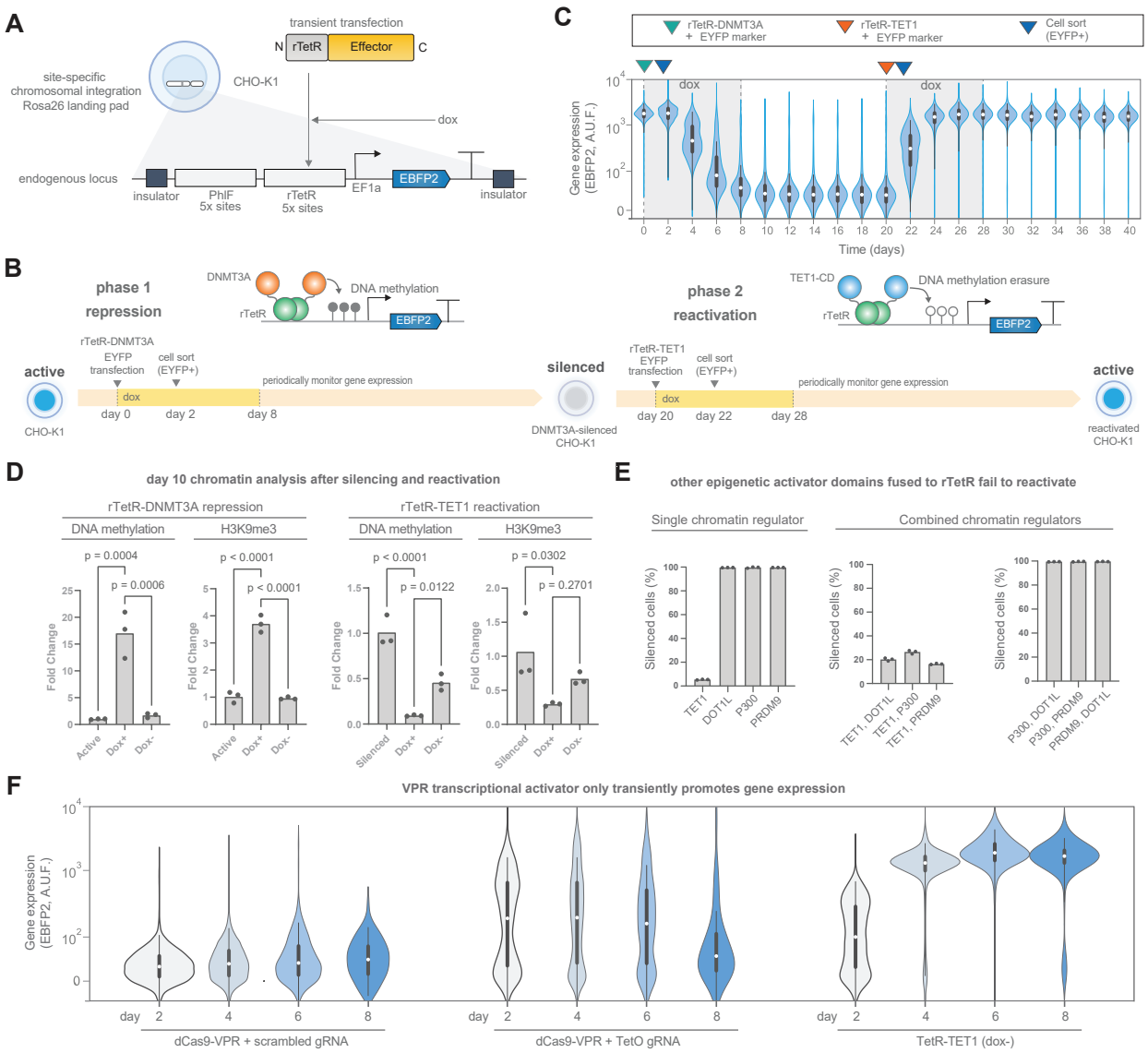

Fig. 1. Targeted chromatin editing enables reversible control of epigenetic and transcriptional state in mammalian somatic cells. Caption on next page.

Targeted chromatin editing enables reversible control of epigenetic and transcriptional state in adult mammalian cells. A. Schematic of the experimental system. The reporter gene is integrated in the ROSA26 locus in CHO-K1 cells. The promoter (hEF1a core + intron) drives expression of EBFP2 and is downstream of binding sites for PhlF and rTetR. The construct is flanked by cHS4 chromatin insulators. 'dox' is doxycycline, a small molecule that enables rTetR operator binding. **B.** Schematic of the experimental workflow for targeted chromatin editing in the engineered CHO-K1 cells. **C.** Violin plots of flow cytometry measurements during CHO-K1 cell state switching by sequential transient rTetR-DNMT3A and rTetR-TET1 transfections. Data shown are from one replicate from three independent replicates. **D.** Quantitative PCR analysis after methylated DNA immunoprecipitation (MeDIP) or CUT&RUN targeting H3K9me3. Bars represent mean values of three independent replicates. Statistics were performed with an ordinary one-way ANOVA with Dunnet correction for multiple comparisons. **E.** Bar graph showing percentage of active cells 4 days after transient transfection with the indicated epigenetic effectors as measured by flow cytometry. Data are presented as mean of three independent replicates. **F.** Violin plots of flow cytometry measurements after recruitment of dCas9-VPR or TetR-TET1 over the course of 8 days. Data are plotted from three independent replicates. In all violin plots, the white dot represents the median, the thick box represents the interquartile range (IQR) and the thin gray line represents 1.5x the IQR.

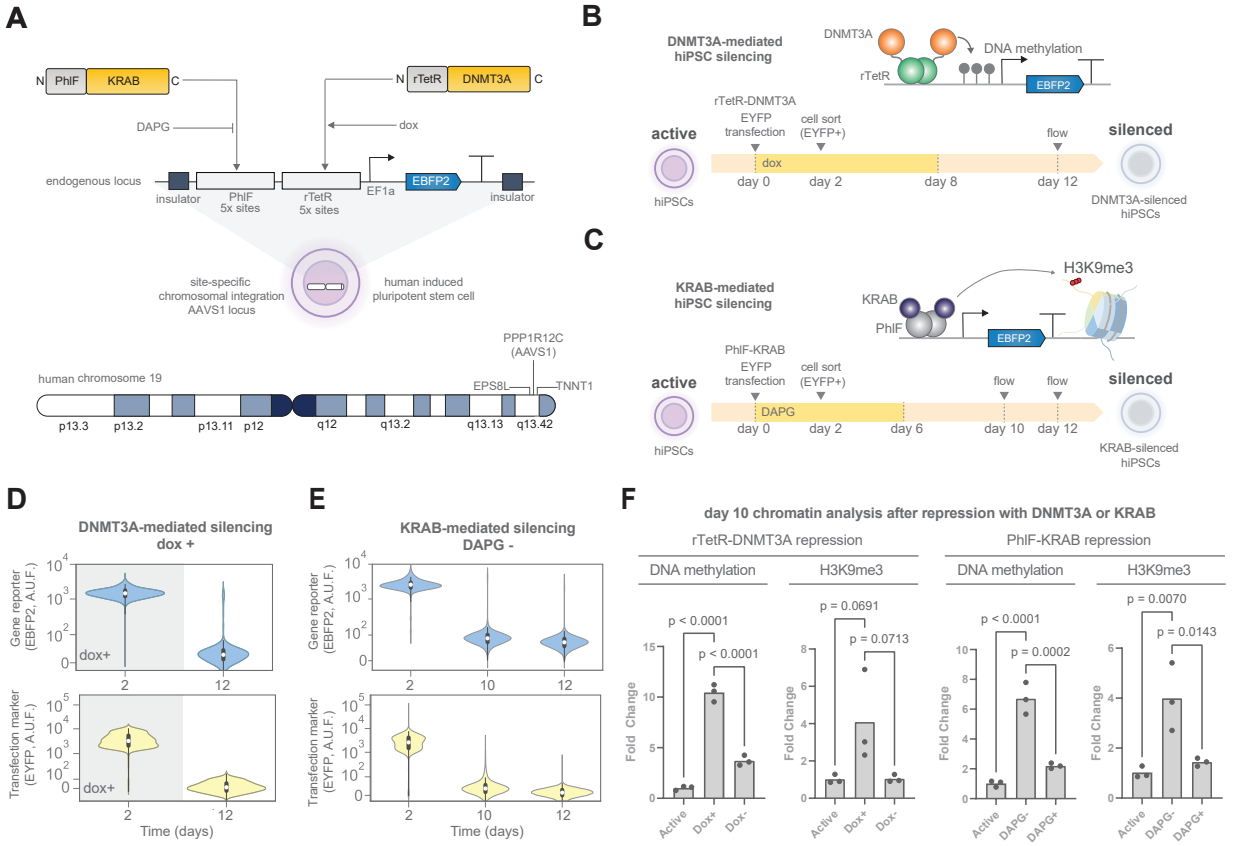

Fig. 2. Different engineered chromatin regulators enable stable silencing in human induced pluripotent stem cells. **A.** Schematic of the experimental system. The reporter system is identical to that used in CHO-K1 cells except that the integration site is the AAVS1 locus in hiPSCs (see Methods and Fig. S4A). 'DAPG' is 2,4-diacetylphloroglucinol, a small molecule that inhibits PhlF binding to its operator. **B-C.** Schematic of the experimental workflow for chromatin editing with **(B)** rTetR-DNMT3A or with **(C)** PhlF-KRAB. **D-E.** Violin plots of flow cytometry measurements after transient **(D)** rTetR-DNMT3A or **(E)** PhlF-KRAB recruitment. Data are plotted from three independent replicates. The white dot represents the median, the thick box represents the interquartile range (IQR) and the thin gray line represents 1.5x the IQR. **F.** Quantitative PCR analysis of chromatin after methylated DNA immunoprecipitation (MeDIP) or CUT&RUN targeting H3K9me3. Bars represent mean values of three independent replicates. Statistics were performed with an ordinary one-way ANOVA with Dunnet correction for multiple comparisons.

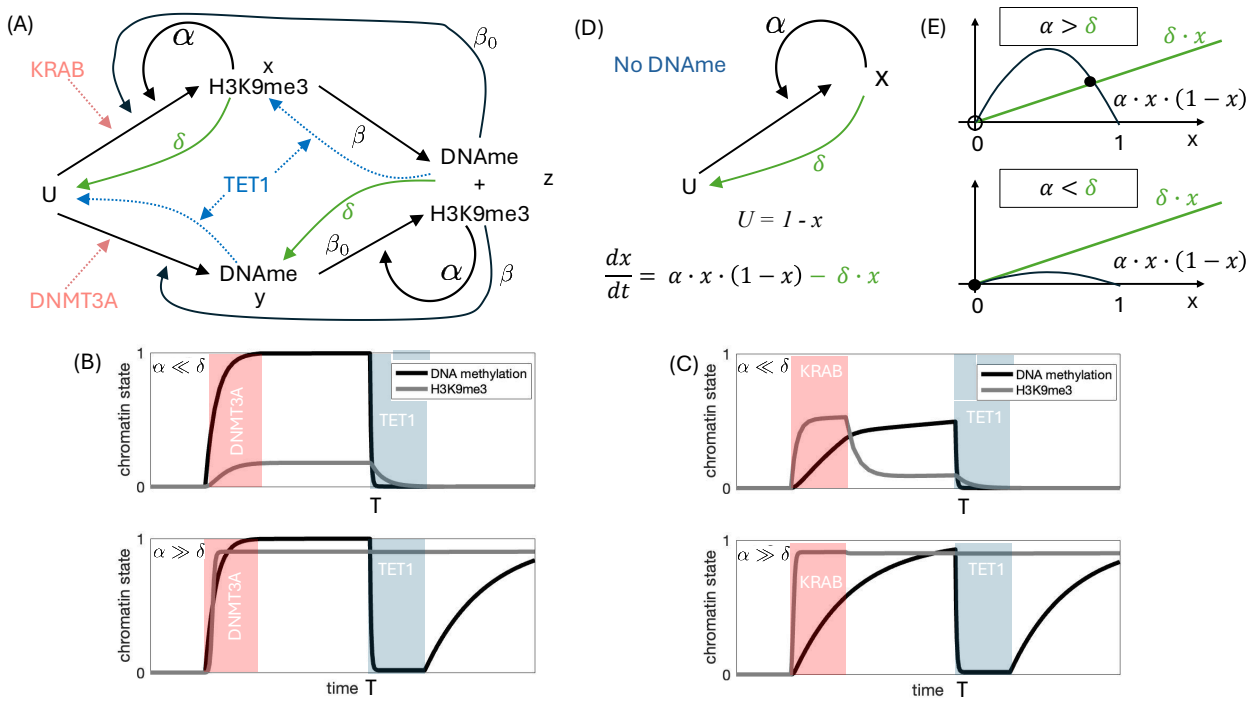

Fig. 3. Model of the positive feedback between DNA methylation and H3K9me3 in hiPSCs. A. Straight arrows depict methylation reactions catalyzed by exogenous chromatin regulators (KRAB and DNMT3A) or by recruitment of endogenous chromatin regulators by other factors as represented by α, β and β_0. The green arrows represent H3K9me3 decay while the blue dashed arrows represent the erasure of DNA methylation through TET1. (U) represents unmodified nucleosomes, (x) represents nucleosomes with H3K9me3, (y) represents nucleosomes with DNA methylation, and (z) represents nucleosomes with both marks. Positive feedback marked by α represents H3K9me3 autocatalysis. Arrows marked by β represent the recruitment of DNA methylation by H3K9me3. Arrows marked by β_0 represent the recruitment of H3K9me3 by DNA methylation. Only some of these recruitment arrows are shown to avoid clutter. **B.** Trajectories of the fraction of H3K9me3 methylation (grey) and DNA methylation (black) after temporary recruitment of DNMT3A followed by temporary recruitment of TET1. **C.** Trajectories of the fraction of H3K9me3 methylation (grey) and DNA methylation (black) after temporary recruitment of KRAB followed by temporary recruitment of TET1. Red shade indicates the timespan of DNMT3A or KRAB recruitment whereas the blue shade indicates the timespan of TET1 recruitment. Computational simulations were performed with the ODE model in Supplementary Text. **D.** In the absence of DNMT3A or KRAB and presence of high TET1 levels, the circuit in panel A reduces to a two-state system devoid of DNA methylation. Here, (U) represents the fraction of unmodified nucleosomes and (x) represents the fraction of H3K9me3-modifed nucleosomes. The ODE represents the rate of change of the fraction of modified nucleosomes, where α represents the strength of H3K9me3 autocatalysis and δ represents its decay constant. **E.** The steady states lie at the intersection of the production rate (black) and decay rate (green) lines. Solid circles represent stable steady states while open circles represent unstable steady states.

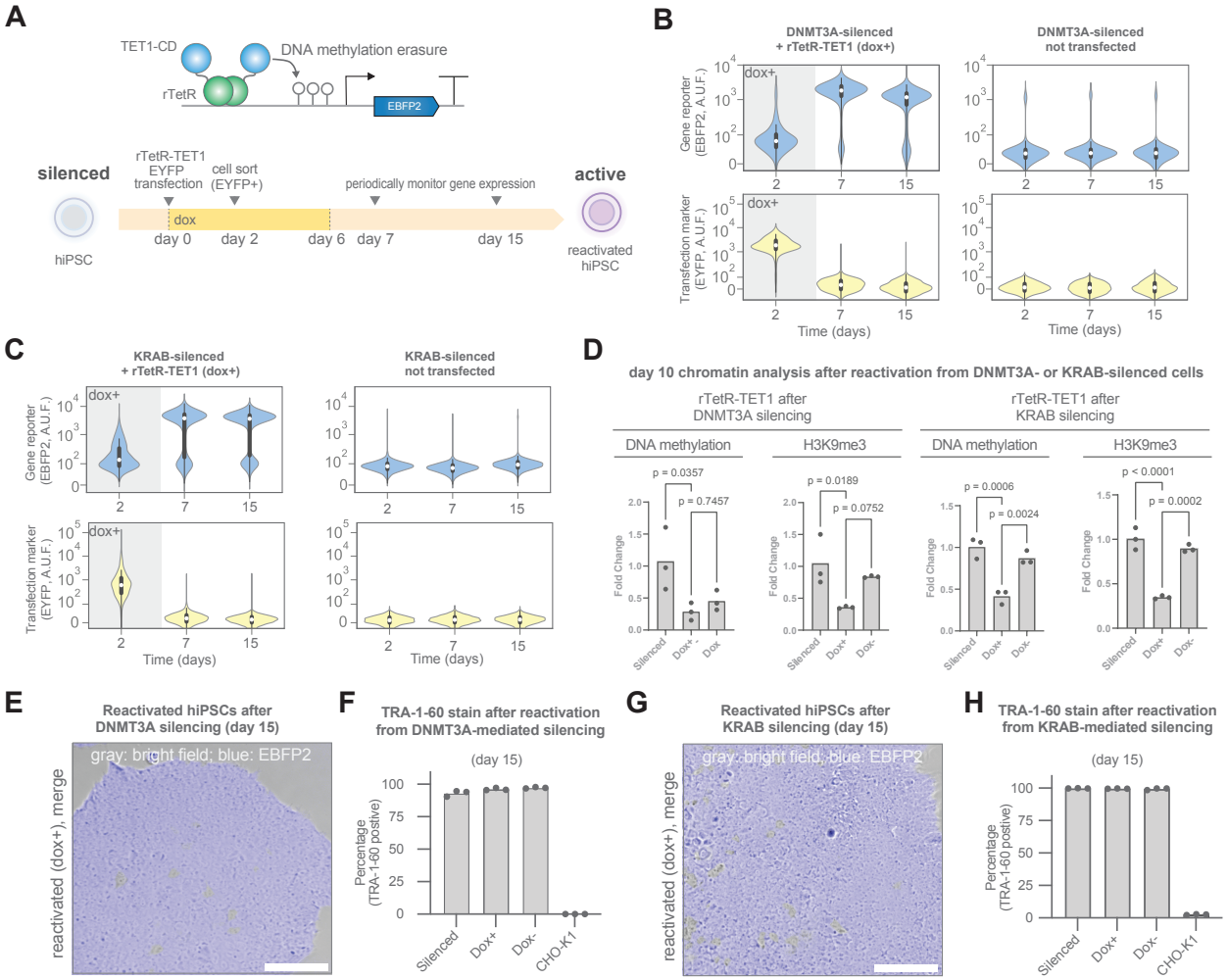

Fig. 4. Targeted chromatin editing with an engineered TET1-based chromatin regulator efficiently reverses targeted silencing in hiPSCs. A. Schematic of the experimental setup for hiPSC reactivation by transient rTetR-TET1 transfection. **B-C.** Violin plots of flow cytometry measurements after rTetR-TET1 transfection of hiPSCs silenced with **(B)** rTetR-DNMT3A or **(C)** PhlF-KRAB. Data are plotted from three independent replicates. The white dot represents the median, the thick box represents the interquartile range (IQR) and the thin gray line represents 1.5x the IQR. **D.** Quantitative PCR analysis (qPCR) of chromatin after methylated DNA immunoprecipitation (MeDIP) or CUT&RUN targeting H3K9me3 (see Methods). Bars represent mean values of three independent replicates. Statistics were performed with an ordinary one-way ANOVA with Dunnet correction for multiple comparisons. **E-F.** Pluripotency assessment by **(E)** colony morphology and **(F)** cell surface marker staining (TRA-1-60) of reactivated cells from DNMT3A-silenced state. **G-H.** Pluripotency assessment by **(G)** colony morphology and **(H)** cell surface marker staining (TRA-1-60) of reactivated cells from KRAB-silenced state.

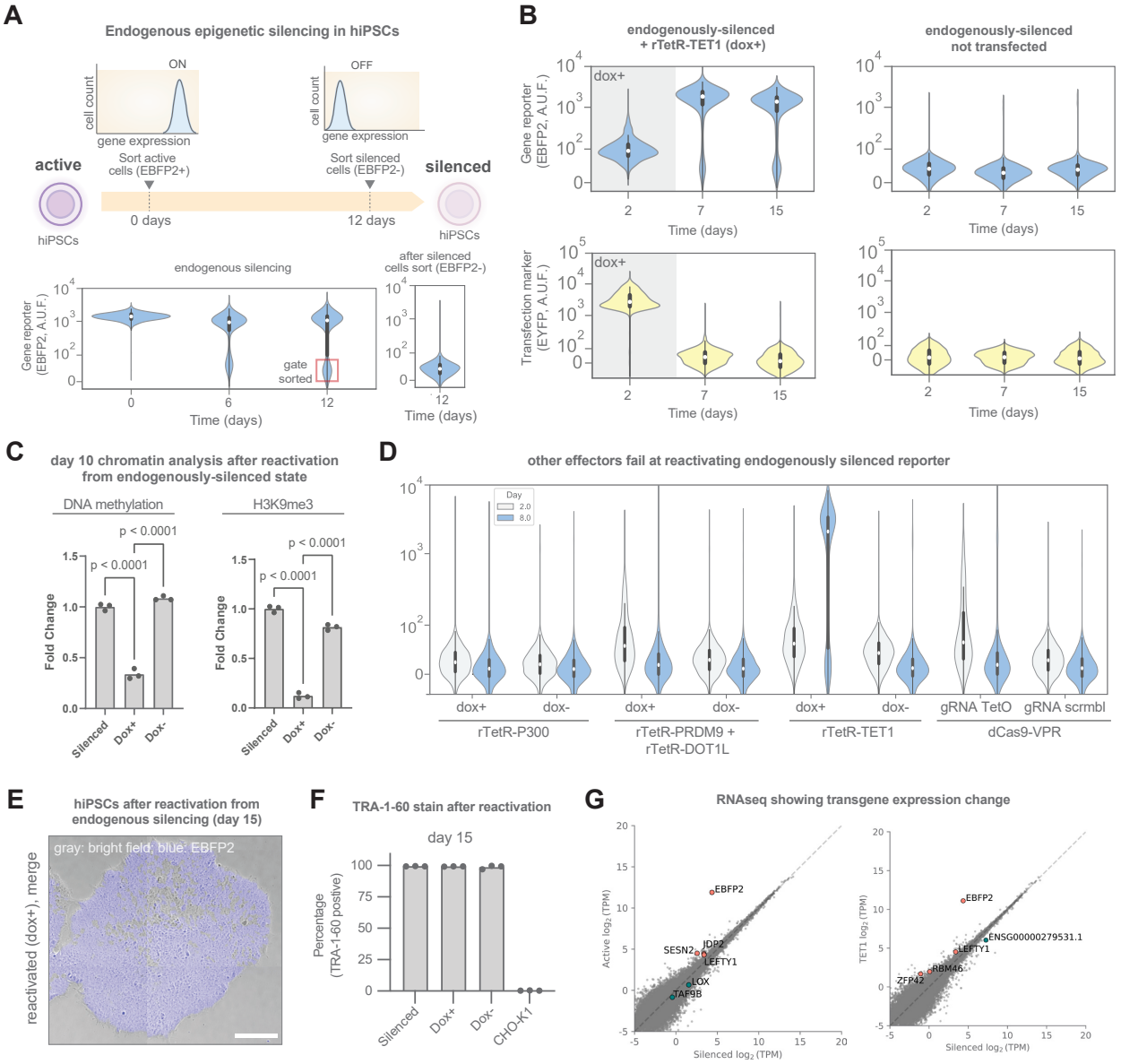

Fig. 5. Endogenous transgene silencing in hiPSCs is efficiently reversed by targeted TET1-mediated demethylation. **A.** Top: Schematic of the experimental setup to obtain endogenously silenced hiPSCs. Bottom: Violin plots of flow cytometry measurements tracking reporter fluorescence. At day 12, non-expressing cells (EBFP2-) were sorted (red gate), expanded and used as starting point for reactivation experiments. **B.** Violin plots of flow cytometry measurements after rTetR-TET1 transfection of endogenously-silenced hiPSCs. Error bars are s.d. of the mean from three independent replicates. **C.** Quantitative PCR analysis (qPCR) of chromatin after methylated DNA immunoprecipitation (MeDIP) or CUT&RUN targeting H3K9me3. Bars represent mean values of three independent replicates. Statistics were performed with an ordinary one-way ANOVA with Dunnet correction for multiple comparisons. **D.** Violin plots of flow cytometry measurements after transfection of endogenously-silenced cells with different epigenetic and transcriptional regulators. Data are plotted from three independent replicates. **E-F.** Pluripotency assessment by **(E)** colony morphology and **(F)** cell surface marker (TRA-1-60) staining of reactivated cells from the endogenously-silenced state. Data are plotted as mean from three independent replicates. **G.** Normalized transcript counts for cells in the active state, endogenously-silenced cells, and reactivated with TET1. TPM: Transcripts per million. For all violin plots, the white dot represents the median, the thick box represents the interquartile range (IQR) and the thin gray line represents 1.5x the IQR.

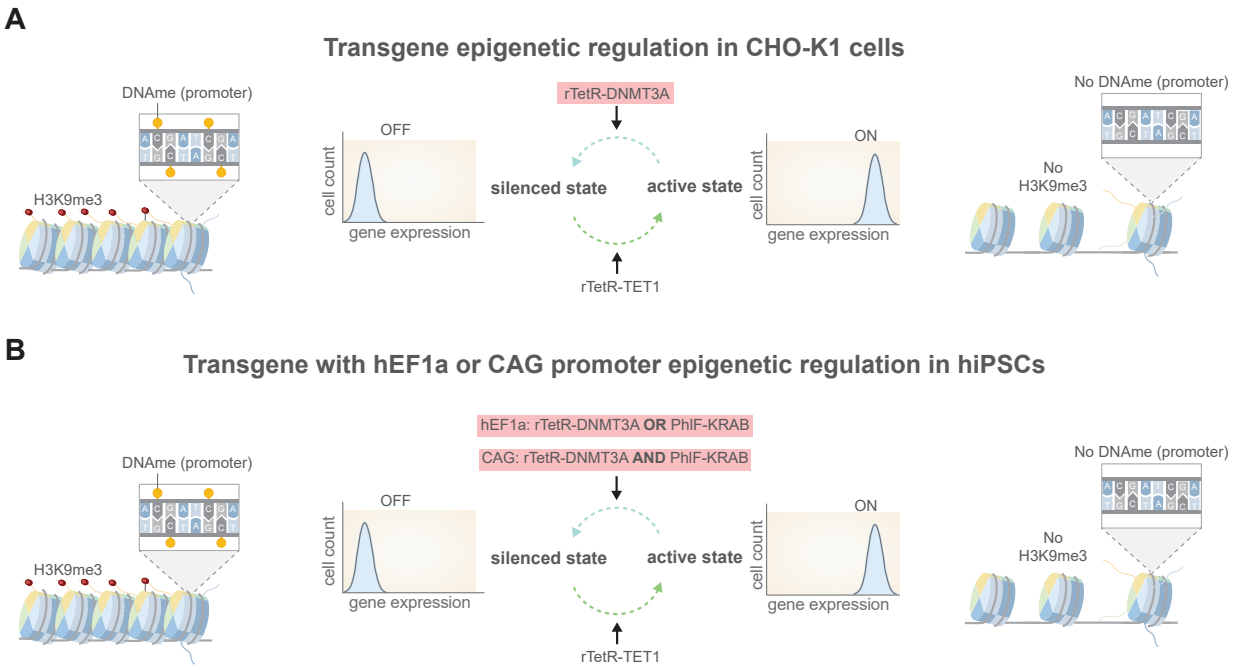

Fig. 6. Schematic showing emergent model for context-dependence of transgene transcriptional control by chromatin editing. A. Model of reversible transgene epigenetic editing in CHO-K1 cells cells. **B.** Model of reversible transgene epigenetic editing in hiPSCs with hEF1 or CAG promoter.

Methods

Cell Culture. All cells were maintained in a humidified incubator at 37℃ with 5% CO2 under sterile conditions. CHO-K1 cells were cultured in tissue culture-treated 10 cm dishes (Corning) in Dulbecco's Modified Eagle Medium (DMEM) (Corning) supplemented with 10% fetal bovine serum (FBS) (Corning), 1X non-essential amino acids (Gibco), and occasionally 100 U/ml penicillin (Sigma), and 100 µg/ml streptomycin (Sigma). Cells were passaged every 2-3 days. For regular passaging, the growth medium was aspirated and the cells were washed with 1X PBS without magnesium or calcium ions (Corning) before adding a sufficient amount of 0.25% trypsin-EDTA (Corning) and incubating at 37℃ in a 5% CO2 incubator for 3-5 minutes to allow cell dissociation. The reaction was subsequently quenched by the addition of 1-2 volumes of complete DMEM. The cell suspension was transferred to 15 mL conical tube and centrifuged at 200 g for 3 minutes. After discarding the supernatant, the cell pellet was resuspended in fresh growth medium. The cell suspension was then diluted at a ratio of 1:10 - 1:20 and transferred to new tissue culture-treated plates with 12-14 mL of fresh complete medium. PGP1 human induced pluripotent stem cells (hiPSCs), generously provided by Prof. George Church at Harvard University, were cultured in mTesR Plus medium (STEMCELL Technologies) occasionally supplemented with 100 U/ml penicillin (Sigma), and 100 µg/ml streptomycin (Sigma). Medium was replaced every day or every other day depending on confluency. Cells were grown in 6-well plates pre-coated with hESC-qualified LDEV-free Matrigel (Corning). To coat the plates, Matrigel was diluted according to the dilution factor of the specific Lot Number in 25 mL of ice-cold DMEM/F12 before dispensing it in the culture plates at 1 mL/well for 6 well plates and 0.5 mL/well for 12-well plates. Plates were sealed with parafilm and stored at 4℃ for up to 2 weeks until needed. Plates required for splitting or seeding were first incubated for at least 1 hour at room temperature or 30 minutes at 37℃ to allow proper coating. Routine passaging of the hiPSCs was conducted every 3-5 days. Briefly, plates were first checked for differentiated regions, which were subsequently marked. Media was aspirated and differentiated regions were scraped off with a pipet tip. The remaining cells were washed with PBS and incubated with 1 mL Gentle Cell Dissociation Reagent (STEMCELL Technologies) for 4-6 minutes at room temperature. After aspirating the dissociation reagent, 1 mL pre-warmed mTeSR Plus medium was added, the colonies were detached using a sterile cell scraper and transferred to 15 mL conical tube and triturated 1-3 times with a 5 mL serological pipet. Finally, 1:10 - 1:40 of the population was reseeded into Matrigel-coated 6 well plates and placed in the incubator at 37℃ with 5% CO2 overnight.

DNA construction. The pX330-U6-Chimeric_BB-CBh-hSpCas9 plasmid used in this study was a gift from Feng Zhang (Addgene plasmid 42230). Target sgRNA sequences for the AAVS1 locus were designed using

Benchling software. The DNA oligonucleotides AAVS1gRNAF and AAVS1-gRNAR were synthesized, annealed, and inserted into the pX330-U6-Chimeric_BB-CBh-hSpCas9 plasmid via Golden Gate assembly. The HDR donor plasmid was cloned by modifying the HDR template using restriction cloning. Sequences for chromatin regulators were cloned by hierarchical golden gate assembly. Briefly, epigenetic regulator sequences bearing kozak sequence and start / stop codons were ordered as gene fragments from Azenta and were flanked by BbsI cleavage sites and a 4bp buffer sequence. The gene fragment was inserted into a gene backbone by golden gate assembly using BbsI and T4 DNA ligase in T4 DNA ligase buffer (NEB) to obtain the level 0 part. The resulting plasmid comprises the epigenetic regulator ORF flanked by BsaI sites for modular cloning. The epigenetic regulator transcriptional unit was cloned by MoClo using the NEBridge GG BsaI Mastermix (NEB) and the resulting level 1 plasmid was purified using a Plasmid MIDI kit (Qiagen). Quantifications were performed using a Nanodrop 2000 after blanking with the supplied Qiagen elution buffer.

Chromatin regulator design. We employed DNA binding domains of TetR, rTetR and PhlF for sequence-specific targeting[109]. Effector domains used in this study include DNMT3A catalytic domain (UniProt Q9Y6K1 [aa602-912]), KRAB domain from ZNF10 (UniProt P21506 [aa11-75]), TET1 catalytic domain (UniProt Q8NFU7 [aa1419-2136]), dCas9-VPR (Addgene 63798), P300 core domain (UniProt Q09472 [aa1048-1664]), DOT1L catalytic domain (UniProt Q8TEK3 [aa1-416]), and PRDM9 catalytic domain (UniProt Q9NQV7 [aa106-413]). The KRAB domain was linked to rTetR or PhlF by GGGGS linker. All other effector domains were linked to DNA binding domain by flexible linker XTEN80 derived from E-XTEN [aa29-108] described by Schellenberger et al.[110]. For nuclear localization, the nuclear localization sequence of the SV40 Large T-antigen (PPKKKRKV) was appended to the C terminal of each regulator. The full length fusion protein sequences are reported in Supplementary Information.

Cell engineering. The CHO-K1 cell line used in this study was previously described in[66]. To generate the hiPSC landing pad cell line (Fig. S4A), hiPSCs (PGP1) were transfected with 1000 ng of total DNA, maintaining a 1:1 ratio between the pX330-U6-Chimeric_BB-CBh-hSpCas9 plasmid with the inserted AAVS1 sgRNA and the donor plasmid. Following transfection, cells were cultured for 10 days in mTesR Plus medium, after which antibiotic selection was initiated by supplementing the medium with 200 µg/ml Hygromycin B (InvivoGen) for two weeks. To generate a single-cell suspension, the cells were incubated with Accutase (STEMCELL Technologies) for 8 minutes in a humidified incubator at 37℃ with 5% CO2. The suspension was then centrifuged at 200 g for 3 minutes, and the resulting cell pellet was resuspended in mTesR medium supplemented with 10 µM Y-27632 and placed on ice. Fluorescence-activated cell sorting (FACS) was performed using a BD FACSAria to isolate EYFP-positive cells. The sorted cells were replated in Matrigel-coated plates in mTesR Plus medium containing 10 µM Y-27632 and 100 U/ml penicillin, 100 µg/ml streptomycin (Corning) for 24 hours, after which the Y-27632

supplement was withdrawn. A clonal cell line was then derived by seeding at clonal density in a Matrigel-coated 10 cm dish (50 cells/cm^2 for 2,000-3,000 cells per dish) in mTesR Plus medium supplemented with 1X CloneR-2 and selecting individual colonies to expand.

For chromosomal integrations into the landing pad (Fig. S4A), hiPSCs bearing the landing pad were transfected with 1000 ng of DNA, maintaining a 1:1 ratio between the Bxb1 constitutive expression vector (CAG:Bxb1) and the reporter plasmid. At 24-48 hours post-transfection, antibiotic selection was initiated by feeding cells with fresh mTesR Plus medium supplemented with 1 µg/ml puromycin (InvivoGen) for a period of 7 days. At Day 10 post-trasnfection, a single-cell suspension was prepared by incubating the cells in Accutase (STEMCELL Technologies) for 8 minutes in a humidified incubator at 37℃ with 5% CO2. The cell suspension was then trasnferred to a 15 mL contical tube and centrifuged at 200 g for 3 minutes, resuspended in mTesR Plus medium supplemented with 10 µM Y-27632 and 1 mg/mL BSA. Fluorescence-activated cell sorting (FACS) was conducted using a BD FACS Aria to isolate EBFP2+/EYFP- cells. Following sorting, the cells were cultured for 24-48 hours in mTesR Plus medium supplmented with 1X CloneR-2, 100 U/ml penicillin and 100 µg/ml streptomycin (Corning). Once viable colonies were visible, Cloner-2 supplement was withdrawn from the medium and the cells were expanded for banking. CHO-K1 cells were frozen as single cells in complete DMEM supplemented with 5% DMSO. PGP1 cells were frozen as aggregates in mFresR (STEMCELL Technologies). Freezing was performed in a Mr. Frosty to obtain a 1 ℃/min cooling rate until -80℃, for a maximum time of 2 weeks short term storage at -80℃. Cells were transferred to a liquid nitrogen freezer for long-term storage.

Transfections. Transfections were carried in 12-well plates. For CHO-K1 cell transfections, they were treated with 0.25% trypsin-EDTA (Corning) and incubated for 3-5 minutes at 37℃ with 5% CO2. Trypsin was neutralized by adding 1-2 volumes of pre-warmed complete growth medium at room temperature and the cell suspension was trasnfered to a 15 mL conical tube and at 200 g for 3 minutes. Then, the supernatant was aspirated and the cells were resuspended in sufficient complete growth medium before performing a viable cell count using Trypan Blue and a Countess (Invitrogen). Cells were seeded in 12-well tissue culture-treated plates (Corning) at a density of 125,000-150,000 cells per well and incubated for 24 hours in an incubator at 37℃ with 5% CO2. The following day, the cells were washed once with 1X PBS and fed fresh growth medium free of antibiotics. Transfections were carried out using Lipofectamine LTX (Invitrogen) according to manufacturer's instructions. Briefly, 800-1000 ng of DNA was combined in 50 µL of Opti-MEM (Gibco) with 1 µL of PLUS reagent in a 1.5 mL tube. Simlarly, 5 µL of Lipofectamine LTX was added to 50 µL of Opti-MEM in another 1.5 mL tube. The solutions were allowed to equilibrate for 5 minutes at room temperature, after which they were combined and incubated a further 5 minutes at room temperature to form the lipofection complexes. After incubation, 100 µL of formed transfection complexes were added dropwise to each well and evenly distributed by shaking. The media and trasnfection complexes were

replaced after 24 hours in an incubator at 37℃ with 5% CO2. For hiPSCs transfections, the cells were washed once with 0.5 mL 1X PBS and incubated in 0.5 mL Accutase (STEMCELL Technologies) for 8 minutes in a humidified incubator at 37℃ with 5% CO2. Following incubation, 0.5 mL pre-warmed DMEM/F12 or PBS was added and the cell suspension was centrifuged at 200 g for 3 minutes, and the pellet was resuspended in an appropriate volume of fresh mTeSR Plus medium supplemented with 10 µM Y-27632 (STEMCELL Technologies) to obtain a single cell suspension. Viable cells were then counted using Trypan Blue and a Countess and seeded at a density 150,000-200,000 cells per well in Matrigel-coated 12-well plates in 1 ml mTeSR Plus supplemented with 10 µM Y-27632 (ROCKi). After 24 hours, Y-27632 was withdrawn from the medium. Transfections were carried out with Lipofectamine Stem (Invitrogen) according to manufacturer's instructions. Briefly, 800-1000 ng of DNA was combined in 50 µL of Opti-MEM (Gibco) 1.5 mL tube. Simlarly, 4 µL of Lipofectamine Stem was added to 50 µL of Opti-MEM in another 1.5 mL tube. The solutions were allowed to equilibrate for 5 minutes at room temperature, after which they were combined and incubated a further 10 minutes at room temperature to form the lipofection complexes. After incubation, 100 µL of formed transfection complexes were added dropwise to each well and evenly distributed by shaking. The media and transfection complexes were replaced after 24 hours in an incubator at 37℃ with 5% CO2.

Cell sorting. CHO-K1 cells were detached by treatment with 0.25% trypsin-EDTA (Corning) at 37℃ in a humidified incubator with 5% CO_2 for 5 minutes. Trypsin was neutralized by the addition of 1 volume of complete growth media at room temperature. The cells were then centrifuged at 200 g for 3 minutes, after which the supernatant was discarded and the cell pellet was resuspended in complete growth media supplemented with 1 mg/ml bovine serum albumin (BSA) and the appropriate small molecules according to the experimental conditions (+/- 2 µM dox). The cell suspension was filtered through a 35 µm filter cap into 5 mL round bottom polystyrene flow cytometry tubes. Fluorescence-activated cell sorting (FACS) was performed using a BD FACS Aria sorter 42-48 hours post-transfection, and 25,000-30,000 cells were collected in complete growth media supplemented with penicillin/streptomycin and the corresponding small molecules. Human iPSCs were detached with Accutase (STEMCELL Technologies) by incubating at 37℃ in a humidified incubator with 5% CO_2 for 7 minutes. The cells were then centrifuged at 200 g for 3 minutes, after which the supernatant was discarded, and the cell pellet was resuspended in mTeSR Plus supplemented with 10 μM Y-27632, 1 mg/ml BSA and the appropriate small molecules according to the experimental conditions (2 µM dox or 30 µM DAPG). The cell suspension was filtered through a 35 µm filter cap into 5 mL polystyrene tubes for flow cytometry. Fluorescence-activated cell sorting (FACS) was performed using a BD FACS Aria sorter 42-48 hours post-transfection, and 25,000-30,000 cells were collected and cultured for 4 days on matrigel-coated plates in mTesR Plus supplemented 1X CloneR-2 (STEMCELL Technologies), penicillin/streptomycin and the corresponding small molecules based on

the experiment. Fluorescence detection of EBFP2 was conducted using a 405 nm laser and a 450/50 filter with a voltage setting of 332 V, while EYFP was measured using a 488 nm laser and a 515/20 filter with a voltage setting of 200 V.

Flow cytometry. CHO-K1 cells were detached by treating them with 0.25% trypsin-EDTA (Corning) and incubating at 37℃ in a 5% CO2 incubator for 5 minutes. The reaction was quenched by adding 1 volume of complete warm growth medium. Cells were transferred to 1.5 mL tubes and centrifuged at 200 g for 3 minutes and the supernatant was aspirated. The resulting cell pellet was resuspended in an adequate volume of 1X PBS or fresh complete growth medium and passed through a 35 µm filter cap into 5 mL polypropylene tubes (Falcon) for flow cytometry analysis. Human iPSCs were detached with Accutase (STEMCELL Technologies) for 7 minutes in a humidified incubator at 37℃ with 5% CO2. Following incubation, 1 volume of 1X PBS or DMEM/F12 was added and the suspension was transferred to 1.5 mL tubes before centrifugation at 200 g for 3 minutes. The supernatant was aspirated and the cell pellet was resuspended in 1X PBS or mTesR Plus medium supplemented with 10 µM Y-27632 and subsequently filtered through a 35 µm filter cap into 5 mL flow cytometry tubes (Falcon). Flow cytometry data was collected on a BD LSRFortessa, with specific laser and filter settings for each fluorophore: EBFP2 was detected using a 405 nm laser and a 450/50 filter at 259 V, EYFP with a 488 nm laser and a 530/30 filter at 190 V. Cytoflow (version 1.2) was utilized for data analysis, including calculating cell densities, means, standard deviations, and percentages from the flow cytometry measurements. The data were gated for single cells based on forward and side scatter, and only gated events were included in subsequent analysis. After data processing in Cytoflow, plots were generated using Cytoflow, GraphPad Prism, or Matplotlib. Bar plots were created using GraphPad Prism.

CHO-K1 cell state switching. For transfections, 500 ng of rTetR-DNMT3A and 300 ng of EYFP were used for repression. Cells were sorted for high EYFP expression on day 2 after transfection and analyzed every 2 days by flow cytometry as described above. For reactivation, 500 ng of rTetR-TET1 and 300 ng of EYFP were used. Sorting and analysis was performed as before. Doxycycline was supplemented to the medium at a final concentration of 2 µM (1.03 µg/mL) for 8 days.

CHO-K1 reactivation with chromatin regulators. For single transfection of a single regulator, 500 ng of the regulator and 300 ng of EYFP transfection marker were used. For co-transfections, 250 ng of either regulator and 300 ng of EYFP were used to maintain a total of 800 ng DNA. Doxycyline (2 µM) was supplemented to the medium for 4 days. Similarly, a 1:1 ratio was maintained between dCas9-VPR (250 ng) and the sgRNA (250 ng), with 300 ng EYFP. Cells were analyzed by flow cytometry as described above and computationally binned for EYFP expression.

hiPSC silencing. For silencing, 500 ng of rTetR-DNMT3A or PhlF-KRAB along with 300 ng EYFP was used. In the case of rTetR-DNMT3A, 2 µM doxycycline was supplemented for 8 days. In the case of PhlF-KRAB, DAPG was added at a final concentration of 30 µM from days 8-12. Cells were sorted for medium high EYFP expression 2 days after transfection and analyzed by flow cytometry as described above.

hiPSC reactivation. Reactivation of silenced hiPSCs was performed with 500 ng of rTetR-TET1 and 300 ng EYFP. Cells were sorted for medium high EYFP expression 2 days after trasnfection and analyzed by flow cytometry as described above.

MeDIP-qPCR. MeDIP was conducted using the MagMeDIP-qPCR kit (Diagenode) following the manufacturer's protocol with minor modifications. Transfections were performed as described above and cells were harvested following 10 days of culture. Genomic DNA was extracted from a confluent well of 12-well plate (approx. 3 million cells) using Monarch gDNA extraction kit (NEB T3010) according to kit instructions. Purified gDNA was eluted in 55 µL heated elution buffer. Quantification was performed on a Nanodrop, and DNA concentration was diluted to 100 ng/µL for those exceeding that value. DNA shearing was carried out in a Bioruptor Pico (Diagenode). For shearing, 50 µL of the DNA dilution was transferred to 0.2 mL Bioruptor tubes and sonicated for 30 cycles with a 30 s ON, 30 s OFF per cycle. Next, 47 µL of sheared DNA was denatured by combining with 10 µL ultrapure water and 33 µL 1X MagMaster Mix for 3 minutes at 95 ℃ according to manufacturer protocol and then cooled quickly on ice for 10 minutes. For antibody-bead binding, 75 µL of denatured sheared DNA was combined with 20 µL of washed MagBeads and 5 µL of antibody mix according to manufacturer protocol. The anti-5mC antibody Clone 33D3 (Diagenode - C15200081) was used. The DNA-bead-antibody solution was rotated overnight at 4 ℃. The following day, beads were washed 4 times with the supplied wash buffers as per instructions (3x 100 µL buffer A, 1x 100 µL buffer B) and the enriched DNA was eluted in 100 µL of DNA isolation buffer supplemented with Proteinase K by incubating for 15 minutes at 55 ℃ then 15 minutes at 100 ℃. The supernatant was recovered from the beads using a magnetic rack and used as input for qPCR reactions. All qPCR reactions were performed in technical duplicates using Power SYBR Green PCR Master Mix (Applied Biosystems) and primers on a LightCycler 96 system (Roche). Reactions consisted of 50 µL final volume, with 10 µL input DNA and 0.4 µM forward and reverse primers. Melt curve analysis was performed to verify a single amplification product, and the LightCycler 96 Application Software (Roche) was used to obtain Ct values. The promoter region of the reporter gene was the target location to be amplified. IgF2 in CHO-K1 and TSH2B in human cells served as reference endogenous genes. The fold changes reported were calculated using the standard $\delta\delta$Ct method. Primer sequences are reported in Supplementary Information.

CUT&RUN-qPCR. CUT&RUN-qPCR was performed according to[111] with minor modifications. Transfections

were performed as described above and cells were harvested following 10 days of culture. Cells were harvested (CHO-K1 cells with 0.25% Trypsin-EDTA for 3-5 minutes, PGP1 cells with Acctuase for 8-10 minutes), washed twice with 0.5 mL 1X PBS by centrifuging at 600 g for 3 minutes and discarding supernatant and finally resuspending in 1 mL PBS. Next, a viable cell count with Trypan blue exclusion was performed and 1 million cells per condition were transferred to fresh 1.5 mL tubes and pelleted by cetrifugation at 600 g for 3 minutes. The resulting pellet was washed twice with 1 mL wash buffer (20 mM HEPES pH 7.5, 150 mM NaCl, 0.5 mM spermidine, 1X EDTA-free protease inhibitor) and resuspended in 990 mL of wash buffer. Meanwhile, 100 µL of Concanavalin A Magnetic beads (Bangs Labs - BP531) were washed three times in 1 mL binding buffer (20 mM HEPES pH 7.5, 20 mM KCl, 1 mM $CaCl_2$, 1 mM $MnCl_2$), and finally resuspended in 100 µL of binding buffer (enough for 9 samples, scale accordingly, 10 µL beads per sample + 10% excess). For cell-bead binding, 10 µL of the washed beads were added to the 990 mL of washed cells and rotated at room temperature for 15 minutes. Next, the supernatant was discarded and the beads-cells were resuspended in 200 µL of antibody buffer (wash buffer + 0.05% digitonin + 2 mM EDTA) and 3 µL of the antibody was added. We used a polyclonal antibody specific to histone 3 lysine 9 trimethylation (H3K9me3) (Active Motif - 39161). The cell-bead-antibody slurry was then transferred to 0.2 mL PCR tubes and rotated overnight at 4 ℃. The following day, the beads were washed twice with 200 µL of digitonin buffer (wash buffer + 0.05% digitonin), then resuspended in 200 µL digitonin buffer and 2.5 µL of pAG-MNase (Active Motif - 53181) was added. The tubes were rotated for 30 mintutes at room temperature. Next, the beads were washed twice with 200 µL of digitonin buffer before being resuspended in 200 µL digitonin buffer and cooled on an aluminum rack on ice for 10 minutes. To initiate chromatin digestion, 2 µL of 0.1 M $CaCl_2$ was added to the cooled bead slurry, combined well and rotated for 4 hours at 4 ℃ in a cold room. Chromatin digestion was terminated by the addition of 67 µL of stop buffer (5 mM NaCl, 20 mM EDTA, 4 mM EGTA, 50 µg/mL RNase A, 50 µg/mL Glycogen). The tubes were then incubated in a thermocycler at 37 ℃ (lid 65 ℃) for 20 minutes, then spun on a tabletop micro-centrifuge, placed on magnetic rack and the supernatant (aprox. 267 µL - sample) was transferred to fresh 2.0 mL tubes for purification with Monarch Spin PCR&DNA cleanup kit (NEB - T1130). Briefly, 5 volumes (1335 µL) of binding buffer were added to the recovered supernatant, passed through the supplied spin tubes by centrifugation, washed twice with 500 µL of 80% ethanol and eluted in 20 µL elution buffer. The eluate was used as the DNA input for qPCR reactions. All qPCR reactions were performed in technical duplicates using Power SYBR Green PCR Master Mix (Applied Biosystems) and primers on a LightCycler 96 system (Roche). Reactions consisted of 50 µL final volume, with 3 µL input DNA and 0.4 µM forward and reverse primers. Melt curve analysis was performed to verify a single amplification product, and the LightCycler 96 Application Software (Roche) was used to obtain Ct values. The promoter region of the reporter gene was the target location to be amplified. IgF2 in CHO-K1 and TSH2B in human cells served as reference endogenous genes. The fold changes reported were calculated using the standard $\delta\delta$Ct method.

Primer sequences are reported in Supplementary Information.

Immunostaining for flow cytometry. Cells were prepared for staining by first incubating them in Accutase (STEM CELL Technologies) for 7 minutes. After incubation, the cells were resuspended in 4 volumes of mTesR medium and centrifuged at 200 g for 3 minutes. The pellet was resuspended in mTeSR containing 10 µM ROCK inhibitor (Y-27632), followed by another centrifugation at 200 g. The cells were then resuspended in phosphate-buffered saline (PBS) and washed twice with PBS, each wash involving centrifugation at 200 g for 3 minutes. Following the final wash, the cells were resuspended in 100 µL of staining solution containing anti-TRA-1-60-AF647 antibody diluted 1:50 in PBS. The staining was performed in a 96-well plate, with tissue culture-treated wells used for human induced pluripotent stem cells (hiPSCs) and non-tissue culture-treated wells for CHO-K1 cells. The cells were incubated overnight for 18 hours at 4℃, protected from light by covering the plates with aluminum foil. The following day, the cells were washed twice with PBS to remove excess antibody, and resuspended in 250 µL of PBS for flow cytometry analysis.

Microscopy. Imaging was performed using a Zeiss Axio Observer Z1 inverted widefield fluorescence microscope equipped with a AxioCam MRm camera and X-Cite Series 120 light source in a humidified chamber at 37 ℃ and 5%CO_2. Images were acquired on ZenPro software with objective A Pln 20x/0.8 DICII in bright field and the EBFP2 fluorescence channel. In total, 9 tiles (3x3 images) were acquired and stitched automatically by the software. Contrast adjustments and merged images were generated with MATLAB.

Bulk RNAseq. Cell seeding, transfection and sorting was performed as described above. In particular, 500 ng of TetR-TET1 and 300 ng EYFP were used for transfection. Sorting was performed 2 days later, and populations in the active state, endogenously -silenced state as well as those with high trasnfection marker were sorted and maintained in culture for 8 days. On day 10, cells were treated with Accutase for 8 mins at 37℃, washed twice with 1X PBS and viable cells were counted. Total RNA was extracted from 3 million cells with the Monarch Spin RNA Isolation Kit (NEB - T2110S) and eluted in 100 µL Ultrapure water before quantification on a Nanodrop. Samples were submitted to the MIT BioMicro Center for sequencing. Briefly, mRNA was enriched with poly-A bead capture, adapters were ligated to form the library and sequencing was performed on a SingularG4 sequencer. Genomic sequences, transcriptomic sequences, and gene annotation files were obtained from GENCODE (release 49). The EBFP2 sequence was then appended to each of the obtained files. Genome indexing and paired-end sequence alignment was performed with bowtie (version 1.2.3)[112]. Aligned sequences were counted using the featureCounts function from the Rsubread R package (version 2.12.3)[113]. Transcriptome indexing and transcript quantification was performed with salmon (version 1.10.0)[114]. Differential expression analyses were performed using DESeq2 (version 1.38.3)[115]. Only genes with at least 10 counts in at least 3 samples were included in the

differential expression analysis.

Computational analysis. All simulations conducted in this paper were done using Gillespie's Stochastic Simulation Algorithm (SSA)[116].

Acknowledgements

We thank the Koch Institute's Flow Cytometry Core at MIT for the support with cell sorting. Furthermore, we would like to thank our funding: NSF-MODULUS (Award number 2027949) and NIH-NIBIB (Award number R56EB036090). We thank the MIT BioMicro Center for their assistance with RNAseq data acquisition and analysis.

Declaration of interests

The authors declare no competing interests.

References

[1] J. B. Black, P. Perez-Pinera, and C. A. Gersbach, "Mammalian synthetic biology: Engineering biological systems," *Annual Review of Biomedical Engineering*, vol. 19, no. Volume 19, 2017, pp. 249–277, 2017. [Online]. Available: https://www.annualreviews.org/content/journals/10.1146/annurev-bioeng-071516-044649

[2] T. Kitada, B. DiAndreth, B. Teague, and R. Weiss, "Programming gene and engineered-cell therapies with synthetic biology," *Science*, vol. 359, no. 6376, p. eaad1067, 2018.

[3] A. Cubillos-Ruiz, T. Guo, A. Sokolovska, P. F. Miller, J. J. Collins, T. K. Lu, and J. M. Lora, "Engineering living therapeutics with synthetic biology," *Nature Reviews Drug Discovery*, vol. 20, pp. 941–960, 2021.

[4] C. J. Bashor, I. B. Hilton, H. Bandukwala, D. M. Smith, and O. Veiseh, "Engineering the next generation of cell-based therapeutics," *Nature Reviews Drug Discovery*, vol. 21, pp. 655–675, 2022.

[5] M. Mathur, J. S. Xiang, and C. D. Smolke, "Mammalian synthetic biology for studying the cell," *Journal of Cell Biology*, vol. 216, no. 1, pp. 73–82, 12 2016. [Online]. Available: https://doi.org/10.1083/jcb.201611002

[6] A. L. Grilo and A. Mantalaris, “The increasingly human and profitable monoclonal antibody market,” *Trends in Biotechnology*, vol. 37, no. 1, pp. 9–16, 2019. [Online]. Available: https://www.sciencedirect.com/science/article/pii/S0167779918301495

[7] R. O’Flaherty, A. Bergin, E. Flampouri, L. M. Mota, I. Obaidi, A. Quigley, Y. Xie, and M. Butler, “Mammalian cell culture for production of recombinant proteins: A review of the critical steps in their biomanufacturing,” *Biotechnology Advances*, vol. 43, p. 107552, 2020. [Online]. Available: https://www.sciencedirect.com/science/article/pii/S0734975020300495

[8] E. A. Kimbrel and R. Lanza, “Next-generation stem cells — ushering in a new era of cell-based therapies,” *Nature Reviews Drug Discovery*, vol. 19, pp. 463–479, 2020.

[9] M. Mansouri and M. Fussenegger, “Therapeutic cell engineering: designing programmable synthetic genetic circuits in mammalian cells,” *Protein & Cell*, vol. 13, no. 7, pp. 476–489, 09 2021. [Online]. Available: https://doi.org/10.1007/s13238-021-00876-1

[10] W. W. Wong and W. A. Lim, “Golden age of immunoengineering,” *Immunological Reviews*, vol. 320, no. 1, pp. 4–9, 2023. [Online]. Available: https://onlinelibrary.wiley.com/doi/abs/10.1111/imr.13283

[11] A. P. Teixeira and M. Fussenegger, “Synthetic gene circuits for regulation of next-generation cell-based therapeutics,” *Advanced Science*, vol. 11, no. 8, p. 2309088, 2024. [Online]. Available: https://advanced.onlinelibrary.wiley.com/doi/abs/10.1002/advs.202309088

[12] M. Fitzgerald, M. Livingston, C. Gibbs, and T. L. Deans, “Rosa26 docking sites for investigating genetic circuit silencing in stem cells,” *Synthetic Biology*, vol. 5, no. 1, p. ysaa014, 08 2020. [Online]. Available: https://doi.org/10.1093/synbio/ysaa014

[13] S. C. Ngai, R. Rosli, A. Al Abbar, and S. Abdullah, “Dna methylation and histone modifications are the molecular lock in lentivirally transduced hematopoietic progenitor cells,” *BioMed Research International*, vol. 2015, no. 1, p. 346134, 2015.

[14] S. Spencer, A. Gugliotta, J. Koenitzer, H. Hauser, and D. Wirth, “Stability of single copy transgene expression in chok1 cells is affected by histone modifications but not by dna methylation,” *Journal of Biotechnology*, vol. 195, pp. 15–29, 2015. [Online]. Available: https://www.sciencedirect.com/science/article/pii/S0168165614010451

[15] N. Veith, H. Ziehr, R. A. MacLeod, and S. M. Reamon-Buettner, “Mechanisms underlying epigenetic and transcriptional heterogeneity in chinese hamster ovary (cho) cell lines,” *BMC biotechnology*, vol. 16, pp. 1–16, 2016.

[16] J. Zimak, Z. W. Wagoner, N. Nelson, B. Waechtler, H. Schlosser, M. Kopecky, J. Wu, and W. Zhao, “Epigenetic silencing directs expression heterogeneity of stably integrated multi-transcript unit genetic circuits,” *Scientific reports*, vol. 11, no. 1, p. 2424, 2021.

[17] M. Seczynska, S. Bloor, S. M. Cuesta, and P. J. Lehner, “Genome surveillance by hush-mediated silencing of intronless mobile elements,” *Nature*, vol. 601, no. 7893, pp. 440–445, 2022.

[18] A. Cabrera, H. I. Edelstein, F. Glykofrydis, K. S. Love, S. Palacios, J. Tycko, M. Zhang, S. Lensch, C. E. Shields, M. Livingston, R. Weiss, H. Zhao, K. A. Haynes, L. Morsut, Y. Y. Chen, A. S. Khalil, W. W. Wong, J. J. Collins, S. J. Rosser, K. Polizzi, M. B. Elowitz, M. Fussenegger, I. B. Hilton, J. N. Leonard, L. Bintu, K. E. Galloway, and T. L. Deans, “The sound of silence: Transgene silencing in mammalian cell engineering,” *Cell Systems*, vol. 13, no. 12, pp. 950–973, 2022.

[19] A. L. Spencley, S. Bar, T. Swigut, R. A. Flynn, C. H. Lee, L.-F. Chen, M. C. Bassik, and J. Wysocka, “Co-transcriptional genome surveillance by hush is coupled to termination machinery,” *Molecular Cell*, vol. 83, no. 10, pp. 1623–1639.e8, 2023. [Online]. Available: https://www.sciencedirect.com/science/article/pii/S109727652300285X

[20] L. Ordovás, L. Ordovas, R. Boon, R. Boon, M. Pistoni, M. Pistoni, Y. Chen, Y. Chen, E. Wolfs, E. Wolfs, W. Guo, W. Guo, R. Sambathkumar, R. Sambathkumar, S. Bobis-Wozowicz, S. Bobis-Wozowicz, S. Bobis-Wozowicz, N. Helsen, N. Helsen, J. Vanhove, J. Vanhove, P. Berckmans, P. Berckmans, Q. Cai, Q. Cai, K. Vanuytsel, K. Vanuytsel, K. Eggermont, K. Eggermont, V. Vanslembrouck, V. Vanslembrouck, B. Z. Schmidt, B. Z. Schmidt, S. Raitano, S. Raitano, L. V. D. Bosch, L. V. D. Bosch, Y. Nahmias, Y. Nahmias, T. Cathomen, T. Cathomen, T. Struys, T. Struys, C. M. Verfaillie, and C. M. Verfaillie, “Efficient recombinase-mediated cassette exchange in hpscs to study the hepatocyte lineage reveals aavs1 locus-mediated transgene inhibition,” *Stem cell reports*, 2015.

[21] J. A. Oyer, A. Chu, S. Brar, and M. S. Turker, “Aberrant epigenetic silencing is triggered by a transient reduction in gene expression,” *PLoS One*, vol. 4, no. 3, p. e4832, 2009.

[22] J. K. K. Mark, C. S. Y. Lim, F. Nordin, and G. J. Tye, “Expression of mammalian proteins for diagnostics and therapeutics: a review,” *Molecular Biology Reports*, vol. 49, no. 11, pp. 10 593–10 608, 2022.

[23] W.-J. Xu, Y. Lin, C.-L. Mi, J.-Y. Pang, and T.-Y. Wang, “Progress in fed-batch culture for recombinant protein production in cho cells,” *Applied microbiology and biotechnology*, vol. 107, no. 4, pp. 1063–1075, 2023.

[24] V. Sifniotis, E. Cruz, B. Eroglu, and V. Kayser, “Current advancements in addressing key challenges

of therapeutic antibody design, manufacture, and formulation," *Antibodies*, vol. 8, no. 2, 2019. [Online]. Available: https://www.mdpi.com/2073-4468/8/2/36

[25] M. Hunter, P. Yuan, D. Vavilala, and M. Fox, "Optimization of protein expression in mammalian cells," *Current protocols in protein science*, vol. 95, no. 1, p. e77, 2019.

[26] J.-H. Zhang, L.-L. Shan, F. Liang, C.-Y. Du, and J.-J. Li, "Strategies and considerations for improving recombinant antibody production and quality in chinese hamster ovary cells," *Frontiers in Bioengineering and Biotechnology*, vol. 10, p. 856049, 2022.

[27] M. Malm, C.-C. Kuo, M. M. Barzadd, A. Mebrahtu, N. Wistbacka, R. Razavi, A.-L. Volk, M. Lundqvist, D. Kotol, H. Tegel, S. Hober, F. Edfors, T. Gräslund, V. Chotteau, R. Field, P. G. Varley, R. G. Roth, N. E. Lewis, D. Hatton, and J. Rockberg, "Harnessing secretory pathway differences between hek293 and cho to rescue production of difficult to express proteins," *Metabolic Engineering*, vol. 72, pp. 171–187, 2022. [Online]. Available: https://www.sciencedirect.com/science/article/pii/S1096717622000441

[28] L. A. Bailey, D. Hatton, R. Field, and A. J. Dickson, "Determination of chinese hamster ovary cell line stability and recombinant antibody expression during long-term culture," *Biotechnology and Bioengineering*, vol. 109, no. 8, pp. 2093–2103, 2012. [Online]. Available: https://analyticalsciencejournals.onlinelibrary.wiley.com/doi/abs/10.1002/bit.24485

[29] J. Chusainow, Y. S. Yang, J. H. Yeo, P. C. Toh, P. Asvadi, N. S. Wong, and M. G. Yap, "A study of monoclonal antibody-producing cho cell lines: What makes a stable high producer?" *Biotechnology and bioengineering*, vol. 102, no. 4, pp. 1182–1196, 2009.

[30] M. Kim, P. M. O'Callaghan, K. A. Droms, and D. C. James, "A mechanistic understanding of production instability in cho cell lines expressing recombinant monoclonal antibodies," *Biotechnology and bioengineering*, vol. 108, no. 10, pp. 2434–2446, 2011.

[31] "The fickle cho: a review of the causes, implications, and potential alleviation of the cho cell line instability problem," *Current Opinion in Biotechnology*, vol. 60, pp. 128–137, 2019.

[32] N. Romanova and T. Noll, "Engineered and natural promoters and chromatin-modifying elements for recombinant protein expression in cho cells," *Biotechnology journal*, vol. 13, no. 3, p. 1700232, 2018.

[33] Y. Zhang, W. Li, T. Laurent, and S. Ding, "Small molecules, big roles – the chemical manipulation of stem cell fate and somatic cell reprogramming," *Journal of Cell Science*, vol. 125, no. 23, pp. 5609–5620, 12 2012. [Online]. Available: https://doi.org/10.1242/jcs.096032

[34] S. M. Chambers, C. A. Fasano, E. P. Papapetrou, M. Tomishima, M. Sadelain, and L. Studer, "Highly efficient neural conversion of human es and ips cells by dual inhibition of smad signaling," *Nature biotechnology*, vol. 27, no. 3, pp. 275–280, 2009.

[35] X. Lian, J. Zhang, S. M. Azarin, K. Zhu, L. B. Hazeltine, X. Bao, C. Hsiao, T. J. Kamp, and S. P. Palecek, "Directed cardiomyocyte differentiation from human pluripotent stem cells by modulating wnt/β-catenin signaling under fully defined conditions," *Nature protocols*, vol. 8, no. 1, pp. 162–175, 2013.

[36] F. Xiao, X. Zhang, S. U. Morton, S. W. Kim, Y. Fan, J. M. Gorham, H. Zhang, P. J. Berkson, N. Mazumdar, Y. Cao *et al.*, "Functional dissection of human cardiac enhancers and noncoding de novo variants in congenital heart disease," *Nature genetics*, vol. 56, no. 3, pp. 420–430, 2024.

[37] L. Wang, W. Xu, S. Zhang, G. C. Gundberg, C. R. Zheng, Z. Wan, K. Mustafina, F. Caliendo, H. Sandt, R. Kamm *et al.*, "Sensing and guiding cell-state transitions by using genetically encoded endoribonuclease-mediated microrna sensors," *Nature Biomedical Engineering*, vol. 8, no. 12, pp. 1730–1743, 2024.

[38] N. B. Wang, A. M. Beitz, and K. Galloway, "Engineering cell fate: Applying synthetic biology to cellular reprogramming," *Current Opinion in Systems Biology*, vol. 24, pp. 18–31, 2020, systems immunology & host-pathogen interaction (2020). [Online]. Available: https://www.sciencedirect.com/science/article/pii/S2452310020300342

[39] P. Saxena, B. C. Heng, P. Bai, M. Folcher, H. Zulewski, and M. Fussenegger, "A programmable synthetic lineage-control network that differentiates human ipscs into glucose-sensitive insulin-secreting beta-like cells," *Nature communications*, vol. 7, no. 1, p. 11247, 2016.

[40] P. Guye, M. R. Ebrahimkhani, N. Kipniss, J. J. Velazquez, E. Schoenfeld, S. Kiani, L. G. Griffith, and R. Weiss, "Genetically engineering self-organization of human pluripotent stem cells into a liver bud-like tissue using gata6," *Nature communications*, vol. 7, no. 1, p. 10243, 2016.

[41] M. L. de Groote, P. J. Verschure, and M. G. Rots, "Epigenetic editing : targeted rewriting of epigenetic marks to modulate expression of selected target genes," *Nucleic Acids Research*, vol. 40, no. 21, pp. 10 596–10 613, 09 2012. [Online]. Available: https://doi.org/10.1093/nar/gks863

[42] C. B. Waryah, C. Moses, M. Arooj, and P. Blancafort, *Zinc Fingers, TALEs, and CRISPR Systems: A Comparison of Tools for Epigenome Editing*. New York, NY: Springer New York, 2018, pp. 19–63. [Online]. Available: https://doi.org/10.1007/978-1-4939-7774-1_2

[43] P. Thakore, J. Black, I. Hilton, and C. Gersbach, "Editing the epigenome: technologies for programmable transcription and epigenetic modulation," *Nat Methods*, vol. 13, no. 2, pp. 127–137, Feb 2016.

[44] X. S. Liu, H. Wu, X. Ji, Y. Stelzer, X. Wu, S. Czauderna, J. Shu, D. Dadon, R. A. Young, and R. Jaenisch, "Editing dna methylation in the mammalian genome," *Cell*, vol. 167, no. 1, pp. 233–247, 2016.

[45] J. K. Nuñez, J. Chen, G. C. Pommier, J. Z. Cogan, J. M. Replogle, C. Adriaens, G. N. Ramadoss, Q. Shi, K. L. Hung, A. J. Samelson, A. N. Pogson, J. Y. S. Kim, A. Chung, M. D. Leonetti, H. Y. Chang, M. Kampmann, B. E. Bernstein, V. Hovestadt, L. A. Gilbert, and J. S. Weissman, "Genome-wide programmable transcriptional memory by crispr-based epigenome editing," *Cell*, vol. 184, no. 9, pp. 2503–2519, 2021.

[46] L. Bintu, J. Yong, Y. E. Antebi, K. McCue, Y. Kazuki, N. Uno, M. Oshimura, and M. B. Elowitz, "Dynamics of epigenetic regulation at the single-cell level," *Science*, 2016. [Online]. Available: https://doi.org/10.1126/science.aab2956

[47] M. A. Cappelluti, V. Mollica Poeta, S. Valsoni, P. Quarato, S. Merlin, I. Merelli, and A. Lombardo, "Durable and efficient gene silencing in vivo by hit-and-run epigenome editing," *Nature*, vol. 627, no. 8003, pp. 416–423, 2024.

[48] C. Policarpi, M. Munafò, S. Tsagkris, V. Carlini, and J. A. Hackett, "Systematic epigenome editing captures the context-dependent instructive function of chromatin modifications," vol. 56, pp. 1168–1180, 2024.

[49] A. Amabile, A. Migliara, P. Capasso, M. Biffi, D. Cittaro, L. Naldini, and A. Lombardo, "Inheritable silencing of endogenous genes by hit-and-run targeted epigenetic editing," *Cell*, vol. 167, no. 1, pp. 219–232.e14, 2016. [Online]. Available: https://www.sciencedirect.com/science/article/pii/S0092867416312363

[50] W. F. Chan, W. F. Chan, H. D. Coughlan, H. D. Coughlan, Y. Chen, Y. Chen, C. R. Keenan, C. R. Keenan, G. K. Smyth, G. K. Smyth, A. C. Perkins, A. C. Perkins, T. M. Johanson, T. M. Johanson, R. S. Allan, and R. S. Allan, "Activation of stably silenced genes by recruitment of a synthetic de-methylating module," *Nature Communications*, 2022.

[51] C. Wilk, C. M. Wilk, L. Effenberg, L. Effenberg, H. Abberger, H. Abberger, L. Steenpass, L. Steenpaß, W. Hansen, W. Hansen, M. Zeschnigk, M. Zeschnigk, C. Kirschning, C. J. Kirschning, C. J. Kirschning, J. Buer, J. Buer, J. Kehrmann, and J. Kehrmann, "Crispr/cas9-mediated demethylation of foxp3-tsdr toward treg-characteristic programming of jurkat t cells." *Cellular Immunology*, 2021.

[52] T. V. Nguyen, T. V. Nguyen, R. Lister, and R. Lister, "Genomic targeting of tet activity for targeted demethylation using crispr/cas9." *Methods of Molecular Biology*, 2021.

[53] X. Cui, X. Cui, C. Zhang, C. Zhang, Z. Xu, Z. Xu, S. Wang, S. Wang, X. Li, X. Li, E. Stringer-Reasor, E. Stringer-Reasor, S. Bae, S. Bae, L. Zeng, L. Zeng, D. Zhao, D. Zhao, R. Liu, R. Liu, L. S. Qi, L. S.

Qi, L. Wang, and L. Wang, “Dual crispr interference and activation for targeted reactivation of x-linked endogenous foxp3 in human breast cancer cells,” *Molecular Cancer*, 2022.

[54] I. B. Hilton, I. B. Hilton, A. D’Ippolito, A. M. D’Ippolito, C. M. Vockley, C. M. Vockley, P. I. Thakore, P. I. Thakore, G. E. Crawford, G. E. Crawford, T. E. Reddy, T. E. Reddy, C. A. Gersbach, and C. A. Gersbach, “Epigenome editing by a crispr-cas9-based acetyltransferase activates genes from promoters and enhancers,” *Nature Biotechnology*, 2015.

[55] C. L. Lo, C.-L. Lo, S. R. Choudhury, S. R. Choudhury, J. Irudayaraj, J. M. K. Irudayaraj, F. Zhou, and F. C. Zhou, “Epigenetic editing of ascl1 gene in neural stem cells by optogenetics,” *Scientific Reports*, 2017.

[56] A. Taghbalout, A. Taghbalout, A. Taghbalout, M. Du, M. Du, N. Jillette, N. Jillette, W. Rosikiewicz, W. Rosikiewicz, W. Rosikiewicz, A. Rath, A. Rath, C. D. Heinen, C. D. Heinen, S. Li, S. Li, S. Li, S. Li, S. Li, A. W. Cheng, A. W. Cheng, and A. W. Cheng, “Enhanced crispr-based dna demethylation by casilio-me-mediated rna-guided coupling of methylcytosine oxidation and dna repair pathways,” *Nature Communications*, 2019.

[57] M. L. Maeder, M. L. Maeder, J. Angstman, J. Angstman, M. E. Richardson, M. E. Richardson, S. J. Linder, S. J. Linder, V. Cascio, V. M. Cascio, S. Q. Tsai, S. Q. Tsai, Q. Ho, Q. H. Ho, Q. H. Ho, J. D. Sander, J. D. Sander, D. Reyon, D. Reyon, B. Bernstein, B. E. Bernstein, J. Costello, J. F. Costello, M. Wilkinson, M. F. Wilkinson, J. Joung, and J. K. Joung, “Targeted dna demethylation and activation of endogenous genes using programmable tale-tet1 fusion proteins,” *Nature Biotechnology*, 2013.

[58] F. Tremblay, Q. Xiong, S. S. Shah, C.-W. Ko, K. Kelly, M. S. Morrison, C. Giancarlo, R. N. Ramirez, E. M. Hildebrand, S. B. Voytek *et al.*, “A potent epigenetic editor targeting human pcsk9 for durable reduction of low-density lipoprotein cholesterol levels,” *Nature Medicine*, pp. 1–10, 2025.

[59] E. N. Neumann, T. M. Bertozzi, E. Wu, F. Serack, J. W. Harvey, P. P. Brauer, C. P. Pirtle, A. Coffey, M. Howard, N. Kamath, K. Lenz, K. Guzman, M. H. Raymond, A. S. Khalil, B. E. Deverman, E. V. Minikel, S. M. Vallabh, and J. S. Weissman, “Brainwide silencing of prion protein by aav-mediated delivery of an engineered compact epigenetic editor,” *Science*, vol. 384, no. 6703, p. ado7082, 2024. [Online]. Available: https://www.science.org/doi/abs/10.1126/science.ado7082

[60] S. R. Choudhury, Y. Cui, K. Lubecka, B. Stefanska, and J. Irudayaraj, “Crispr-dcas9 mediated tet1 targeting for selective dna demethylation at brca1 promoter,” *Oncotarget*, vol. 7, no. 29, pp. 46 545–46 556, 2016. [Online]. Available: https://www.oncotarget.com/article/10234/

[61] J. Qian, X. Guan, B. Xie, C. Xu, J. Niu, X. Tang, C. H. Li, H. M. Colecraft, R. Jaenisch, and X. S. Liu, "Multiplex epigenome editing of mecp2 to rescue rett syndrome neurons," *Science Translational Medicine*, vol. 15, no. 679, p. eadd4666, 2023. [Online]. Available: https://www.science.org/doi/abs/10.1126/scitranslmed.add4666

[62] X. S. Liu, H. Wu, M. Krzisch, X. Wu, J. Graef, J. Muffat, D. Hnisz, C. H. Li, B. Yuan, C. Xu, Y. Li, D. Vershkov, A. Cacace, R. A. Young, and R. Jaenisch, "Rescue of fragile x syndrome neurons by dna methylation editing of the fmr1 gene," *Cell*, vol. 172, no. 5, pp. 979–992.e6, 2018. [Online]. Available: https://www.sciencedirect.com/science/article/pii/S0092867418300497

[63] D. Rohm, J. B. Black, S. R. McCutcheon, A. Barrera, S. S. Berry, D. J. Morone, X. Nuttle, C. E. de Esch, D. J. Tai, M. E. Talkowski *et al.*, "Activation of the imprinted prader-willi syndrome locus by crispr-based epigenome editing," *Cell Genomics*, vol. 5, no. 2, 2025.

[64] N. Gödecke, L. Zha, S. Spencer, S. Behme, P. Riemer, M. Rehli, H. Hauser, and D. Wirth, "Controlled reactivation of epigenetically silenced tet promoter-driven transgene expression by targeted demethylation," *Nucleic acids research*, vol. 45, no. 16, pp. e147–e147, 2017.

[65] N. Godecke, S. Herrmann, V. Weichelt, and D. Wirth, "A ubiquitous chromatin opening element and dna demethylation facilitate doxycycline-controlled expression during differentiation and in transgenic mice," *ACS Synthetic Biology*, vol. 12, no. 2, pp. 482–491, 2023.

[66] S. Palacios, S. Bruno, R. Weiss, E. Salibi, I. Goodchild-Michelman, A. Kane, K. Ilia, and D. Del Vecchio, "Analog epigenetic memory revealed by targeted chromatin editing," *Cell Genomics*, 2025.

[67] Y. Ma, M. W. Budde, J. Zhu, and M. B. Elowitz, "Tuning methylation-dependent silencing dynamics by synthetic modulation of cpg density," *ACS Synthetic Biology*, vol. 12, no. 9, pp. 2536–2545, 2023.

[68] R. S. Guerra-Resendez, S. L. Lydon, A. J. Ma, G. C. Bedford, D. R. Reed, S. Kim, E. R. Terán, T. Nishiguchi, M. Escobar, A. R. DiNardo *et al.*, "Characterization of rationally designed crispr/cas9-based dna methyltransferases with distinct methyltransferase and gene silencing activities in human cell lines and primary human t cells," *ACS Synthetic Biology*, 2025.

[69] M. Okano, S. Xie, and E. Li, "Cloning and characterization of a family of novel mammalian dna (cytosine-5) methyltransferases," *Nature genetics*, vol. 19, no. 3, pp. 219–220, 1998.

[70] N. Davidsohn, J. Beal, S. Kiani, A. Adler, F. Yaman, Y. Li, Z. Xie, and R. Weiss, "Accurate predictions of genetic circuit behavior from part characterization and modular composition," *ACS Synthetic Biology*, vol. 4, no. 6, pp. 673–681, 2015, pMID: 25369267. [Online]. Available: https://doi.org/10.1021/sb500263b

[71] J. J. Gam, B. DiAndreth, R. D. Jones, J. Huh, and R. Weiss, “A ‘poly-transfection’ method for rapid, one-pot characterization and optimization of genetic systems,” *Nucleic Acids Research*, vol. 47, no. 18, pp. e106–e106, 08 2019. [Online]. Available: https://doi.org/10.1093/nar/gkz623

[72] J. F. Margolin, J. R. Friedman, W. K. Meyer, H. Vissing, H. J. Thiesen, and F. J. Rauscher, 3rd, “Krüppel-associated boxes are potent transcriptional repression domains,” *Proc. Natl. Acad. Sci.*, vol. 91, no. 10, pp. 4509–4513, 1994. [Online]. Available: 10.1073/pnas.91.10.4509

[73] D. Cano-Rodriguez, R. A. F. Gjaltema, L. J. Jilderda, P. Jellema, J. Dokter-Fokkens, M. H. J. Ruiters, and M. G. Rots, “Writing of h3k4me3 overcomes epigenetic silencing in a sustained but context-dependent manner,” *Nature communications*, vol. 7, no. 1, p. 12284, 2016.

[74] A. Chavez, J. Scheiman, S. Vora, B. W. Pruitt, M. Tuttle, E. PR Iyer, S. Lin, S. Kiani, C. D. Guzman, D. J. Wiegand *et al.*, “Highly efficient cas9-mediated transcriptional programming,” *Nature methods*, vol. 12, no. 4, pp. 326–328, 2015.

[75] B. E. Low, V. Hosur, S. Lesbirel, and M. V. Wiles, “Efficient targeted transgenesis of large donor dna into multiple mouse genetic backgrounds using bacteriophage bxb1 integrase,” *Scientific Reports*, vol. 12, no. 1, p. 5424, 2022.

[76] L. Gaidukov, L. Wroblewska, B. Teague, T. Nelson, X. Zhang, Y. Liu, K. Jagtap, S. Mamo, W. A. Tseng, A. Lowe, J. Das, K. Bandara, S. Baijuraj, N. M. Summers, T. K. Lu, L. Zhang, and R. Weiss, “A multi-landing pad DNA integration platform for mammalian cell engineering,” *Nucleic Acids Res.*, vol. 46, no. 8, pp. 4072–4086, May 2018.

[77] J. R. Smith, S. Maguire, L. A. Davis, M. Alexander, F. Yang, S. Chandran, C. Ffrench-Constant, and R. A. Pedersen, “Robust, persistent transgene expression in human embryonic stem cells is achieved with aavs1-targeted integration,” *Stem cells*, vol. 26, no. 2, pp. 496–504, 2008.

[78] L. Ordovás, R. Boon, M. Pistoni, Y. Chen, E. Wolfs, W. Guo, R. Sambathkumar, S. Bobis-Wozowicz, N. Helsen, J. Vanhove, P. Berckmans, Q. Cai, K. Vanuytsel, K. Eggermont, V. Vanslembrouck, B. Z. Schmidt, S. Raitano, L. Van Den Bosch, Y. Nahmias, T. Cathomen, T. Struys, and C. M. Verfaillie, “Efficient recombinase-mediated cassette exchange in hpscs to study the hepatocyte lineage reveals aavs1 locus-mediated transgene inhibition,” *Stem Cell Reports*, vol. 5, no. 5, pp. 918–931, 2015. [Online]. Available: https://www.sciencedirect.com/science/article/pii/S2213671115002660

[79] D. Klatt, E. Cheng, D. Hoffmann, G. Santilli, A. J. Thrasher, C. Brendel, and A. Schambach, “Differential

transgene silencing of myeloid-specific promoters in the aavs1 safe harbor locus of induced pluripotent stem cell-derived myeloid cells," *Human Gene Therapy*, vol. 31, no. 3-4, pp. 199–210, 2020.

[80] J. R. Bhagwan, E. Collins, D. Mosqueira, M. Bakar, B. B. Johnson, A. Thompson, J. G. Smith, and C. Denning, "Variable expression and silencing of crispr-cas9 targeted transgenes identifies the aavs1 locus as not an entirely safe harbour," *F1000Research*, vol. 8, p. 1911, 2020.

[81] S. Wunderlich, A. Haase, S. Merkert, K. Jahn, M. Deest, H. Frieling, S. Glage, W. Korte, A. Martens, A. Kirschning *et al.*, "Targeted biallelic integration of an inducible caspase 9 suicide gene in ipscs for safer therapies," *Molecular Therapy Methods & Clinical Development*, vol. 26, pp. 84–94, 2022.

[82] Y. Luo, C. Liu, T. Cerbini, H. San, Y. Lin, G. Chen, M. S. Rao, and J. Zou, "Stable enhanced green fluorescent protein expression after differentiation and transplantation of reporter human induced pluripotent stem cells generated by aavs1 transcription activator-like effector nucleases," *Stem cells translational medicine*, vol. 3, no. 7, pp. 821–835, 2014.

[83] S. Bruno, R. J. Williams, and D. Del Vecchio, "Epigenetic cell memory: The gene's inner chromatin modification circuit," *PLOS Computational Biology*, vol. 18, no. 4, pp. 1 – 27, 2022. [Online]. Available: https://doi.org/10.1371/journal.pcbi.1009961

[84] F. Fuks, P. J. Hurd, D. Wolf, X. Nan, A. P. Bird, and T. Kouzarides, "The methyl-cpg-binding protein mecp2 links dna methylation to histone methylation," *J Biol Chem*, vol. 278, no. 6, pp. 4035–4040, 2003. [Online]. Available: https://doi.org/10.1074/jbc.M210256200

[85] E. Hervouet, P. Peixoto, R. Delage-Mourroux, M. Boyer-Guittaut, and P.-F. Cartron, "Specific or not specific recruitment of dnmts for dna methylation, an epigenetic dilemma," *Clin Epigenetics*, no. 10, p. 17, 2018. [Online]. Available: https://doi.org/10.1186/s13148-018-0450-y

[86] L. Lopez-Serra and M. Esteller, "Proteins that bind methylated dna and human cancer: reading the wrong words," *Br J Cancer*, vol. 98, no. 12, pp. 1881–1885, 2008. [Online]. Available: https://doi.org/10.1038/sj.bjc.6604374

[87] N. A. Hathaway, O. Bell, C. Hodges, E. L. Miller, D. S. Neel, and G. R. Crabtree, "Dynamics and memory of heterochromatin in living cells," *Cell*, vol. 149, no. 7, pp. 1447–1460, 2012. [Online]. Available: https://doi.org/10.1016/j.cell.2012.03.052

[88] M. Trerotola, V. Relli, P. Simeone, and S. Alberti, "Epigenetic inheritance and the missing heritability," *Hum Genomics*, vol. 9, no. 1, p. 17, 2015. [Online]. Available: https://doi.org/10.1186/s40246-015-0041-3

[89] T. Zhang, S. Cooper, and N. Brockdorff, “The interplay of histone modifications - writers that read,” *EMBO Rep*, vol. 16, no. 11, pp. 1467–1481, 2015. [Online]. Available: https://doi.org/10.15252/embr.201540945

[90] E. Li and Y. Zhang, “Dna methylation in mammals,” *Cold Spring Harb Perspect Biol*, vol. 6, no. 5, 2014. [Online]. Available: https://doi.org/10.1101/cshperspect.a019133

[91] M. Jackson, A. Krassowska, N. Gilbert, T. Chevassut, L. Forrester, J. Ansell, and B. Ramsahoye, “Severe global dna hypomethylation blocks differentiation and induces histone hyperacetylation in embryonic stem cells,” *Mol Cell Biol*, vol. 24, no. 20, 2004. [Online]. Available: https://doi.org/10.1128/MCB.24.20.8862-8871

[92] W. M. Schopperle and W. C. DeWolf, “The tra-1-60 and tra-1-81 human pluripotent stem cell markers are expressed on podocalyxin in embryonal carcinoma,” *Stem cells*, vol. 25, no. 3, pp. 723–730, 2007.

[93] M.-Y. Son, H. Choi, Y.-M. Han, and Y. Sook Cho, “Unveiling the critical role of rex1 in the regulation of human stem cell pluripotency,” *Stem cells*, vol. 31, no. 11, pp. 2374–2387, 2013.

[94] M. Zabala, N. A. Lobo, J. Antony, L. S. Heitink, G. S. Gulati, J. Lam, N. Parashurama, K. Sanchez, M. Adorno, S. S. Sikandar *et al.*, “Lefty1 is a dual-smad inhibitor that promotes mammary progenitor growth and tumorigenesis,” *Cell Stem Cell*, vol. 27, no. 2, pp. 284–299, 2020.

[95] B. Qian, Y. Li, R. Yan, S. Han, Z. Bu, J. Gong, B. Zheng, Z. Yuan, S. Ren, Q. He *et al.*, “Rna binding protein rbm46 regulates mitotic-to-meiotic transition in spermatogenesis,” *Science advances*, vol. 8, no. 34, p. eabq2945, 2022.

[96] L. M. Johnson, M. Bostick, X. Zhang, E. Kraft, I. Henderson, J. Callis, and S. E. Jacobsen, “The sra methylcytosine-binding domain links dna and histone methylation,” *Current Biology*, vol. 17, no. 4, pp. 379–384, 2007.

[97] J. Zhang, Q. Gao, P. Li, X. Liu, Y. Jia, W. Wu, J. Li, S. Dong, H. Koseki, and J. Wong, “S phase-dependent interaction with dnmt1 dictates the role of uhrf1 but not uhrf2 in dna methylation maintenance,” *Cell research*, vol. 21, no. 12, pp. 1723–1739, 2011.

[98] N. Nady, A. Lemak, J. R. Walker, G. V. Avvakumov, M. S. Kareta, M. Achour, S. Xue, S. Duan, A. Allali-Hassani, X. Zuo *et al.*, “Recognition of multivalent histone states associated with heterochromatin by uhrf1 protein,” *Journal of Biological Chemistry*, vol. 286, no. 27, pp. 24 300–24 311, 2011.

[99] X. Kong, J. Chen, W. Xie, S. M. Brown, Y. Cai, K. Wu, D. Fan, Y. Nie, S. Yegnasubramanian, R. L. Tiedemann *et al.*, “Defining uhrf1 domains that support maintenance of human colon cancer dna methylation and oncogenic properties,” *Cancer cell*, vol. 35, no. 4, pp. 633–648, 2019.

[100] M. Choudalakis, G. Kungulovski, R. Mauser, P. Bashtrykov, and A. Jeltsch, “Refined read-out: The huhrf1 tandem-tudor domain prefers binding to histone h3 tails containing k4me1 in the context of h3k9me2/3,” *Protein Science*, vol. 32, no. 9, p. e4760, 2023.

[101] M. A. Mandegar, N. Huebsch, E. B. Frolov, E. Shin, A. Truong, M. P. Olvera, A. H. Chan, Y. Miyaoka, K. Holmes, C. I. Spencer *et al.*, “Crispr interference efficiently induces specific and reversible gene silencing in human ipscs,” *Cell stem cell*, vol. 18, no. 4, pp. 541–553, 2016.

[102] S. Morita, S. Morita, H. Noguchi, H. Noguchi, T. Horii, T. Horii, K. Nakabayashi, K. Nakabayashi, M. Kimura, M. Kimura, K. Okamura, K. Okamura, A. Sakai, A. Sakai, A. Sakai, H. Nakashima, H. Nakashima, K. Hata, K. Hata, K. Nakashima, K. Nakashima, I. Hatada, I. Hatada, and I. Hatada, “Targeted dna demethylation in vivo using dcas9-peptide repeat and scfv-tet1 catalytic domain fusions,” *Nature Biotechnology*, 2016.

[103] M. Seczynska and P. J. Lehner, “The sound of silence: mechanisms and implications of hush complex function,” *Trends in Genetics*, vol. 39, no. 4, pp. 251–267, 2023.

[104] J. M. C. Danac, R. E. Matthews, A. Gungi, C. Qin, H. Parsons, R. Antrobus, R. T. Timms, and I. A. Tchasovnikarova, “Competition between two hush complexes orchestrates the immune response to retroelement invasion,” *Molecular Cell*, vol. 84, no. 15, pp. 2870–2881, 2024.

[105] H. O’Geen, C. Ren, C. M. Nicolet, A. A. Perez, J. Halmai, V. M. Le, J. P. Mackay, P. J. Farnham, and D. J. Segal, “dcas9-based epigenome editing suggests acquisition of histone methylation is not sufficient for target gene repression,” *Nucleic Acids Res.*, vol. 45, no. 17, pp. 9901–9916, Sep. 2017.

[106] H. O’Geen, H. O’Geen, S. L. Bates, S. L. Bates, S. S. Carter, S. S. Carter, K. A. Nisson, K. A. Nisson, J. Halmai, J. Halmai, K. D. Fink, K. D. Fink, S. K. Rhie, S. K. Rhie, P. Farnham, P. J. Farnham, D. J. Segal, and D. J. Segal, “Ezh2-dcas9 and krab-dcas9 enable engineering of epigenetic memory in a context-dependent manner,” *Epigenetics & Chromatin*, 2019.

[107] Z. Wang, R. Fan, A. Russo, F. M. Cernilogar, A. Nuber, S. Schirge, I. Shcherbakova, I. Dzhilyanova, E. Ugur, T. Anton *et al.*, “Dominant role of dna methylation over h3k9me3 for iap silencing in endoderm,” *Nature Communications*, vol. 13, no. 1, p. 5447, 2022.

[108] A. Tatarakis, H. Saini, J. Yu, W. Feng, C. A. Pinzon-Arteaga, and D. Moazed, “Requirements for establishment and epigenetic stability of mammalian heterochromatin,” *Molecular cell*, vol. 85, no. 18, pp. 3388–3406, 2025.

[109] B. C. Stanton, V. Siciliano, A. Ghodasara, L. Wroblewska, K. Clancy, A. C. Trefzer, J. D. Chesnut, R. Weiss, and C. A. Voigt, "Systematic transfer of prokaryotic sensors and circuits to mammalian cells," *ACS Synth. Biol.*, vol. 3, no. 12, pp. 880–891, Dec. 2014.

[110] V. Schellenberger, C.-w. Wang, N. C. Geething, B. J. Spink, A. Campbell, W. To, M. D. Scholle, Y. Yin, Y. Yao, O. Bogin *et al.*, "A recombinant polypeptide extends the in vivo half-life of peptides and proteins in a tunable manner," *Nature biotechnology*, vol. 27, no. 12, pp. 1186–1190, 2009.

[111] A. Panday, R. Elango, N. A. Willis, and R. Scully, "A modified cut&run-seq technique for qpcr analysis of chromatin-protein interactions," *STAR protocols*, vol. 3, no. 3, p. 101529, 2022.

[112] B. Langmead, C. Trapnell, M. Pop, and S. L. Salzberg, "Ultrafast and memory-efficient alignment of short dna sequences to the human genome," *Genome biology*, vol. 10, no. 3, p. R25, 2009.

[113] Y. Liao, G. K. Smyth, and W. Shi, "The r package rsubread is easier, faster, cheaper and better for alignment and quantification of rna sequencing reads," *Nucleic acids research*, vol. 47, no. 8, pp. e47–e47, 2019.

[114] R. Patro, G. Duggal, M. I. Love, R. A. Irizarry, and C. Kingsford, "Salmon provides fast and bias-aware quantification of transcript expression," *Nature methods*, vol. 14, no. 4, pp. 417–419, 2017.

[115] M. I. Love, W. Huber, and S. Anders, "Moderated estimation of fold change and dispersion for rna-seq data with deseq2," *Genome biology*, vol. 15, no. 12, p. 550, 2014.

[116] D. T. Gillespie, "Stochastic simulation of chemical kinetics," *Annual Review of Physical Chemistry*, vol. 58, no. 1, pp. 35–55, 2007. [Online]. Available: https://doi.org/10.1146/annurev.physchem.58.032806.104637

Supplementary Information (SI)

1 Supplementary Text

Chromatin modification model with DNA methylation and H3K9me3.

In this section, we describe the chemical reaction and ODE model corresponding to the reaction diagram of Fig. 3, which describes the interactions between DNA methylation and H3K9me3 consistent with our data and with the literature. To this end, we represent by U nucleosomes devoid of both DNA methylation and H3K9me3, we let x represent nucleosomes modified with H3K9me3 only, y nucleosomes modified with DNA methylation only, and z nucleosomes modified with both H3K9me3 and DNA methylation. We further let K denote the KRAB input, which recruits enzymes that write H3K9me3, let D represent DNMT3A, and let T represent the TET1 enzyme. With these definitions, the chemical reactions corresponding to the reaction diagram are as follows.

The establishment of H3K9me3 occurs either *de novo* through K or through the autocatalysis by nucleosomes that have H3K9me3[87–89]:

$$\mathrm{U} + \mathrm{K} \xrightarrow{k} \mathrm{x} + \mathrm{K},\ \mathrm{y} + \mathrm{K} \xrightarrow{k} \mathrm{z} + \mathrm{K},\ \mathrm{U} + \mathrm{x} \xrightarrow{\alpha} \mathrm{x} + \mathrm{x},\ \ \mathrm{y} + \mathrm{x} \xrightarrow{\alpha} \mathrm{z} + \mathrm{x},\ \ \mathrm{U} + \mathrm{z} \xrightarrow{\alpha} \mathrm{x} + \mathrm{z},\ \ \mathrm{y} + \mathrm{z} \xrightarrow{\alpha} \mathrm{z} + \mathrm{z}.$$

Additionally, in our experiments H3K9me3 can be brought about by DNA methylation (Fig. 2F), which is consistent with the literature reporting that DNA methylation recruits writers of H3K9me3[84]. To account for this in our model, we add reactions where nucleosomes with DNA methylation (y or z) recruit H3K9me3 on histones devoid of it (U and y):

$$\mathrm{U} + \mathrm{y} \xrightarrow{\beta_0} \mathrm{x} + \mathrm{y},\ \mathrm{U} + \mathrm{z} \xrightarrow{\beta_0} \mathrm{x} + \mathrm{z},\ \mathrm{y} \xrightarrow{\beta_0} \mathrm{z},\ \mathrm{y} + \mathrm{z} \xrightarrow{\beta_0} \mathrm{z} + \mathrm{z},\ \mathrm{y} + \mathrm{y} \xrightarrow{\beta_0} \mathrm{z} + \mathrm{y}.$$

The establishment of DNA methylation also occurs through two different pathways, that is, *de novo* establishment through D on nucleosomes devoid of DNA methylation (U and x):

$$\mathrm{U} + \mathrm{D} \xrightarrow{d} \mathrm{y} + \mathrm{D},\ \mathrm{x} + \mathrm{D} \xrightarrow{d} \mathrm{z} + \mathrm{D},$$

or via the recruitment of DNMT3s by H3K9me3 (x or z) to histones lacking DNA methylation (U or x), consistent with our data (Fig. 2F) and the literature[85,86]:

$$\mathrm{U} + \mathrm{x} \xrightarrow{\beta} \mathrm{y} + \mathrm{x},\ \mathrm{U} + \mathrm{z} \xrightarrow{\beta} \mathrm{y} + \mathrm{z},\ \mathrm{x} \xrightarrow{\beta} \mathrm{z},\ \mathrm{x} + \mathrm{z} \xrightarrow{\beta} \mathrm{z} + \mathrm{z},\ \mathrm{x} + \mathrm{x} \xrightarrow{\beta} \mathrm{z} + \mathrm{x}.$$

Finally, we have the decay of H3K9me3, with rate constant δ:

$$\mathrm{x} \xrightarrow{\delta} \mathrm{U},\ \mathrm{z} \xrightarrow{\delta} \mathrm{y},$$

and the decay of DNA methylation, which is non-negligible only in the presence of the TET1 enzyme T, consistent with our data (Fig. 2F) and the literature[90,91]:

$$\mathrm{y} + \mathrm{T} \xrightarrow{t} \mathrm{U} + \mathrm{T},\ \mathrm{z} + \mathrm{T} \xrightarrow{t} \mathrm{x} + \mathrm{T}.$$

We let x denote the fraction of nucleosomes with H3K9me3, y the fraction of nucleosomes with DNA methylation, z the fraction of nucleosomes with both modifications, and u the fraction of nucleosomes with no modifications. By lumping the t, k, and d rate constants into the level of inputs T for TET1, K for KRAB, and D for DNMT3A, we obtain the following system of ordinary differential equations (ODEs) describing the rate of change of these fractions:

$$\begin{aligned}
\frac{dx}{dt} &= K \cdot u + \alpha \cdot (x+z) \cdot u + \beta_0 \cdot (y+z) \cdot u - \beta \cdot x - \beta \cdot (z+x) \cdot x - D \cdot x - \delta \cdot x + T \cdot z \\
\frac{dy}{dt} &= D \cdot u + \beta \cdot (x+z) \cdot u + \delta \cdot z - \beta_0 \cdot y - \beta_0 \cdot (y+z) \cdot y - \alpha \cdot (x+z) \cdot y - K \cdot y - T \cdot y \\
\frac{dz}{dt} &= D \cdot x + K \cdot y + \alpha \cdot (x+z) \cdot y + \beta_0 \cdot y + \beta_0 \cdot y \cdot (y+z) + \beta \cdot x + \beta \cdot x \cdot (x+z) - T \cdot z - \delta \cdot z
\end{aligned}$$

in which $u = 1 - x - y - z$. The total amount of H3K9me3 $\bar{x} = x + z$ obeys the differential equation:

$$\frac{d\bar{x}}{dt} = K \cdot u + \alpha \cdot \bar{x} \cdot (u+y) + \beta_0 \cdot (y+z) \cdot (u+y) - D \cdot x + D \cdot x + K \cdot y + \beta_0 \cdot y - \delta \cdot \bar{x}.$$

When T is very large and no inputs D or K are present, $y \approx 0$ and $z \approx 0$, which leads to the simplified $\bar{x}$ dynamics as:

$$\frac{d\bar{x}}{dt} = \alpha \cdot \bar{x} \cdot u - \delta \cdot \bar{x},$$

in which $\bar{x} \approx x$ and $u \approx 1 - x$, which is the same ODE as in Fig. 3B. The simulations in Fig. 3DE are obtained with the following parameter values: $\alpha = \{0.1, 10\}$, $\beta = 0.1$, $\beta_0 = 0.1$, $\delta = 1$, $T = 10$, $D = 1$, and $K = 1$. Note that we have let β and β_0 to be smaller than α in the simulations. In fact, if these two parameters are too large, the full system's positive feedback around H3K9me3 and DNA methylation will cause a small residual DNA methylation to push up H3K9me3 levels, which in turn will re-establish DNA methylation, and, similarly, small residual H3K9me3 can push up DNA methylation levels, which re-establish H3K9me3 (Fig. S6AB).

2 Supplementary Tables

Name	Sequence
rTetR-XTEN80-DNMT3A	MSRLDKSKVINGALELLNGVGIEGLTTRKLAQKLGVEQPTLYWHVKNKRALLDALPIEMLDRHHTHFCPLEGESWQDFLRNNAKSYRCALLSHRDGAKVHLGTRPTE KQYETLENQLAFLCQQGFSLENALYALSAVGHFTLGCVLEEQEHQVAKEERETPTTDSMPPLLRQAIELFDRQGAEPAFLFGLELIICGLEKQLKCESGGPSSGAPPP SGGSPAGSPTSTEEGTSESATPESGPGTSTEPSEGSAPGSPAGSPTSTEEGTSTEPSEGSAPGTSTEPSEPSRLQMFFANNHDQEFDPPKVYPPVPAEKRKPIRVL SLFDGIATGLLVLKDLGIQVDRYIASEVCEDSITVGMVRHQGKIMYVGDVRSVTQKHIQEWGPFDLVIGGSPCNDLSIVNPARKGLYEGTGRLFFEFYRLLHDARPKEG DDRPFFWLFENVVAMGVSDKRDISRFLESNPVMIDAKEVSAAHRARYFWGNLPGMNRPLASTVNDKLELQECLEHGRIAKFSKVRTITTRSNSIKQGKDQHFPVFMN EKEDILWCTEMERVFGFPVHYTDVSNMSRLARQRLLGRSWSVPVIRHLFAPLKEYFACVPPKKKRKV
PhlF-KRAB	MARTPSRSSIGSLRSPHTHKAILTSTIEILKECGYSGLSIESVARRAGASKPTIYRWWTNKAALIAEVYENESEQVRKFPDLGSFKADLDFLLRNLWKVWRETICGEAFR CVIAEAQLDPATLTQLKDQFMERRREMPKKLVENAISNGELPKDTNRELLLDMIFGFCWYRLLTEQLTVEQDIEEFTFLLINGVCPGTQRGGGGSASRTLVTFKDVFVD FTREEWKLLDTAQQIVYRNVMLENYKNLVSLGYQLTKPDVILRLEKGEEPWLVPPKKKRKV
rTetR-XTEN80-TET1	MSRLDKSKVINGALELLNGVGIEGLTTRKLAQKLGVEQPTLYWHVKNKRALLDALPIEMLDRHHTHFCPLEGESWQDFLRNNAKSYRCALLSHRDGAKVHLGTRPTE KQYETLENQLAFLCQQGFSLENALYALSAVGHFTLGCVLEEQEHQVAKEERETPTTDSMPPLLRQAIELFDRQGAEPAFLFGLELIICGLEKQLKCESGGPSSGAPPP SGGSPAGSPTSTEEGTSESATPESGPGTSTEPSEGSAPGSPAGSPTSTEEGTSTEPSEGSAPGTSTEPSELPTCSCLDRVIQKDKGPYYTHLGAGPSVAAVREIMEN RYGQKGNAIRIEIVVYTGKEGKSSHGCPIAKWVLRRSSDEEKVLCLVRQRTGHHCPTAVMVVLIMVWDGIPLPMADRLYTELTENLKSYNGHPTDRRCTLNENRTCT CQGIDPETCGASFSFGCSWSMYFNGCKFGRSPSPRRFRIDPSSPLHEKNLEDNLQSLATRLAPIYKQYAPVAYQNQVEYENVARECRLGSKEGRPFSGVTACLDFC AHPHRDIHNMNNGSTVVCTLTREDNRSLGVIPQDEQLHVLPLYKLSDTDEFGSKEGMEAKIKSGAIEVLAPRRKKRTCFTQPVPRSGKKRAAMMTEVLAHKIRAVEKK PIPRIKRKNNSTTTNNSKPSSLPTLGSNTETVQPEVKSETEPHFILKSSDNTKTYSLMPSAPHPVKEASPGFSWSPKTASATPAPLKNDATASCGFSERSSTPHCTMP SGRLSGANAAAADGPGISQLGEVAPLPTLSAPVMEPLINSEPSTGVTEPLTPHQPNHQPSFLTSPQDLASSPMEEDEQHSEADEPPSDEPLSDDPLSPAEEKLPHIDE YWSDSEHIFLDANIGGVAIAPAHGSVLIECARRELHATTPVEHPNRNHPTRLSLVFYQHKNLNKPQHGFELNKIKFEAKEAKNKKMKASEQKDQAANEGPEQSSEVNE LNQIPSHKALTLTHDNVVTVSPYALTHVAGPYNHWVPPKKKRKV
TetR-XTEN80-TET1	MSRLDKSKVINSALELLNEVGIEGLTTRKLAQKLGVEQPTLYWHVKNKRALLDALAIEMLDRHHTHFCPLEGESWQDFLRNNAKSFRCALLSHRDGAKVHLGTRPTEK QYETLENQLAFLCQQGFSLENALYALSAVGHFTLGCVLEDQEHQVAKEERETPTTDSMPPLLRQAIELFDHQGAEPAFLFGLELIICGLEKQLKCESGSGGPSSGAPP PSGGSPAGSPTSTEEGTSESATPESGPGTSTEPSEGSAPGSPAGSPTSTEEGTSTEPSEGSAPGTSTEPSELPTCSCLDRVIQKDKGPYYTHLGAGPSVAAVREIME NRYGQKGNAIRIEIVVYTGKEGKSSHGCPIAKWVLRRSSDEEKVLCLVRQRTGHHCPTAVMVVLIMVWDGIPLPMADRLYTELTENLKSYNGHPTDRRCTLNENRTC TCQGIDPETCGASFSFGCSWSMYFNGCKFGRSPSPRRFRIDPSSPLHEKNLEDNLQSLATRLAPIYKQYAPVAYQNQVEYENVARECRLGSKEGRPFSGVTACLDF CAHPHRDIHNMNNGSTVVCTLTREDNRSLGVIPQDEQLHVLPLYKLSDTDEFGSKEGMEAKIKSGAIEVLAPRRKKRTCFTQPVPRSGKKRAAMMTEVLAHKIRAVEK KPIPRIKRKNNSTTTNNSKPSSLPTLGSNTETVQPEVKSETEPHFILKSSDNTKTYSLMPSAPHPVKEASPGFSWSPKTASATPAPLKNDATASCGFSERSSTPHCTM PSGRLSGANAAAADGPGISQLGEVAPLPTLSAPVMEPLINSEPSTGVTEPLTPHQPNHQPSFLTSPQDLASSPMEEDEQHSEADEPPSDEPLSDDPLSPAEEKLPHID EYWSDSEHIFLDANIGGVAIAPAHGSVLIECARRELHATTPVEHPNRNHPTRLSLVFYQHKNLNKPQHGFELNKIKFEAKEAKNKKMKASEQKDQAANEGPEQSSEVN ELNQIPSHKALTLTHDNVVTVSPYALTHVAGPYNHWVPPKKKRKV
rTetR-KRAB	MSRLDKSKVINGALELLNGVGIEGLTTRKLAQKLGVEQPTLYWHVKNKRALLDALPIEMLDRHHTHFCPLEGESWQDFLRNNAKSYRCALLSHRDGAKVHLGTRPTE KQYETLENQLAFLCQQGFSLENALYALSAVGHFTLGCVLEEQEHQVAKEERETPTTDSMPPLLRQAIELFDRQGAEPAFLFGLELIICGLEKQLKCESGGGGSASRTL VTFKDVFVDFTREEWKLLDTAQQIVYRNVMLENYKNLVSLGYQLTKPDVILRLEKGEEPWLVPPKKKRKV
rTetR-XTEN80-P300	MSRLDKSKVINGALELLNGVGIEGLTTRKLAQKLGVEQPTLYWHVKNKRALLDALPIEMLDRHHTHFCPLEGESWQDFLRNNAKSYRCALLSHRDGAKVHLGTRPTE KQYETLENQLAFLCQQGFSLENALYALSAVGHFTLGCVLEEQEHQVAKEERETPTTDSMPPLLRQAIELFDRQGAEPAFLFGLELIICGLEKQLKCESGGPSSGAPPP SGGSPAGSPTSTEEGTSESATPESGPGTSTEPSEGSAPGSPAGSPTSTEEGTSTEPSEGSAPGTSTEPSEIFKPEELRQALMPTLEALYRQDPESLPFRQPVDPQLL GIPDYFDIVKSPMDLSTIKRKLDTGQYQEPWQYVDDIWLMFNNAWLYNRKTSRVYKYCSKLSEVFEQEIDPVMQSLGYCCGRKLEFSPQTLCCYGKQLCTIPRDATY YSYQNRYHFCEKCFNEIQGESVSLGDDPSQPQTTINKEQFSKRKNDTLDPELFVECTECGRKMHQICVLHHEIIWPAGFVCDGCLKKSARTRKENKFSAKRLPSTRL GTFLENRVNDFLRRQNHPESGEVTVRVVHASDKTVEVKPGMKARFVDSGEMAESFPYRTKALFAFEEIDGVDLCFFGMHVQEYGSDCPPPNQRRVYISYLDSVHFF RPKCLRTAVYHEILIGYLEYVKKLGYTTGHIWACPPSEGDDYIFHCHPPDQKIPKPKRLQEWYKKMLDKAVSERIVHDYKDIFKQATEDRLTSAKELPYFEGDFWPNVL EESIKELEQEEEERKREENTSNESTDVTKGDSKNAKKKNNKKTSKNKSSLSRGNKKKPGMPNVSNDLSQKLYATMEKHKEVFFVIRLIAGPAANSLPPIVDPDPLIPCD LMDGRDAFLTLARDKHLEFSSLRRAQWSTMCMLVELHTQSQDPPKKKRKV
rTetR-XTEN80-PRDM9	MSRLDKSKVINGALELLNGVGIEGLTTRKLAQKLGVEQPTLYWHVKNKRALLDALPIEMLDRHHTHFCPLEGESWQDFLRNNAKSYRCALLSHRDGAKVHLGTRPTE KQYETLENQLAFLCQQGFSLENALYALSAVGHFTLGCVLEEQEHQVAKEERETPTTDSMPPLLRQAIELFDRQGAEPAFLFGLELIICGLEKQLKCESGGPSSGAPPP SGGSPAGSPTSTEEGTSESATPESGPGTSTEPSEGSAPGSPAGSPTSTEEGTSTEPSEGSAPGTSTEPSEMALRVEQRKHQKGMPKASFSNESSLKELSRTANLLN ASGSEQAQKPVSPSGEASTSGQHSRLKLELRKKETERKMYSLRERKGHAYKEVSEPQDDDYLYCEMCQNFFIDSCAAHGPPTFVKDSAVDKGHPNRSALSLPPGL RIGPSGIPQAGLGVWNEASDLPLGLHFGPYEGRITEDEEAANNGYSWLITKGRNCYEYVDGKDKSWANWMRYVNCARDDEEQNLVAFQYHRQIFYRTCRVIRPGCE LLVWYGDEYGQELGIKWGSKWKKELMAGREPKPEIHPCPSCCLAFSSQKFLSQHVERNHSSPPKKKRKV
rTetR-XTEN80-DOT1L	MSRLDKSKVINGALELLNGVGIEGLTTRKLAQKLGVEQPTLYWHVKNKRALLDALPIEMLDRHHTHFCPLEGESWQDFLRNNAKSYRCALLSHRDGAKVHLGTRPTE KQYETLENQLAFLCQQGFSLENALYALSAVGHFTLGCVLEEQEHQVAKEERETPTTDSMPPLLRQAIELFDRQGAEPAFLFGLELIICGLEKQLKCESGGPSSGAPPP SGGSPAGSPTSTEEGTSESATPESGPGTSTEPSEGSAPGSPAGSPTSTEEGTSTEPSEGSAPGTSTEPSEMGEKLELRLKSPVGAEPAVYPWPLPVYDKHHDAAH EIIETIRWVCEEIPDLKLAMENYVLIDYDTKSFESMQRLCDKYNRAIDSIHQLWKGTTQPMKLNTRPSTGLLRHILQQVYNHSVTDPEKLNNYEPFSPEVYGETSFDLVA QMIDEIKMTDDDLFVDLGSGVGQVVLQVAAATNCKHHYGVEKADIPAKYAETMDREFRKWMKWYGKKHAEYTLERGDFLSEEWRERIANTSVIFVNNFAFGPEVDH QLKERFANMKEGGRIVSSKPFAPLNFRINSRNLSDIGTIMRVVELSPLKGSVSWTGKPVSYYLHTIDRTILENYFSSLKNPKLREEQEAARRRQQRESKSNAATPTKGP EGKVAGPADAPMDSGAEEEKAGAATVKKPSPSKARKKKLNKKGRKMAGRKRGRPKKPPKKKRKV

Table 1: Chromatin regulator sequences.

Name	Sequence
hEF1a	TAATTGGCTCCGGTGCCCGTCAGTGGGCAGAGCGCACATCGCCCACAGTCCCCGAGAAGTTGTGGGGAGGGGTCGGCAATTGAACCGGTGCCTAGAGAAGGTGGCGCGGGGTAAACT GGGAAAGTGATGTCGTGTACTGGCTCCGCCTTTTTCCCGAGGGTGGGGGAGAACCGTATATAAGTGCAGTAGTCGCCGTGAACGTTCTTTTTCGCAACGGGTTTGCCGCCAGAACACAG GTAAGTGCCGTGTGTGGTTCCCGCGGGCCTGGCCTCTTTACGGGTTATGGCCCTTGCGTGCCTTGAATTACTTCCACCTGGCTGCAGTACGTGATTCTTGATCCCGAGCTTCGGGTTGGA AGTGGGTGGGAGAGTTCGAGGCCTTGCGCTTAAGGAGCCCCTTCGCCTCGTGCTTGAGTTGAGGCCTGGCCTGGGCGCTGGGGCCGCCGCGTGCGAATCTGGTGGCACCTTCGCGCC TGTCTCGCTGCTTTCGATAAGTCTCTAGCCATTTAAAATTTTTGATGACCTGCTGCGACGCTTTTTTTCTGGCAAGATAGTCTTGTAAATGCGGGCCAAGATCTGCACACTGGTATTTCGGT TTTTGGGGCCGCGGGCGGCGACGGGGCCCGTGCGTCCCAGCGCACATGTTCGGCGAGGCGGGGCCTGCGAGCGCGGCCACCGAGAATCGGACGGGGGTAGTCTCAAGCTGGCCGG CCTGCTCTGGTGCCTGGCCTCGCGCCGCCGTGTATCGCCCCGCCCTGGGCGGCAAGGCTGGCCCGGTCGGCACCAGTTGCGTGAGCGGAAAGATGGCCGCTTCCCGGCCCTGCTGC AGGGAGCTCAAAATGGAGGACGCGGCGCTCGGGAGAGCGGGCGGGTGAGTCACCCACACAAAGGAAAAGGGCCTTTCCGTCCTCAGCCGTCGCTTCATGTGACTCCACGGAGTACCG GGCGCCGTCCAGGCACCTCGATTAGTTCTCGAGCTTTTGGAGTACGTCGTCTTTAGGTTGGGGGGAGGGGTTTTATGCGATGGAGTTTCCCCACACTGAGTGGGTGGAGACTGAAGTTA GGCCAGCTTGGCACTTGATGTAATTCTCCTTGGAATTTGCCCTTTTTGAGTTTGGATCTTGGTTCATTCTCAAGCCTCAGACAGTGGTTCAAAGTTTTTTTCTTCCATTTCAGGTGGATCCC
CAG	CGTTACATAACTTACGGTAAATGGCCCGCCTGGCTGACCGCCCAACGACCCCCGCCCATTGACGTCAATAATGACGTATGTTCCCATAGTAACGCCAATAGGGACTTTCCATTGACGTCA ATGGGTGGAGTATTTACGGTAAACTGCCCACTTGGCAGTACATCAAGTGTATCATATGCCAAGTACGCCCCCTATTGACGTCAATGACGGTAAATGGCCCGCCTGGCATTATGCCCAGTA CATGACCTTATGGGACTTTCCTACTTGGCAGTACATCTACGTATTAGTCATCGCTATTACCATGGTCGAGGTGAGCCCCACGTTCTGCTTCACTCTCCCCATCTCCCCCCCCTCCCCACCC CCAATTTTGTATTTATTTATTTTTTAATTATTTTGTGCAGCGATGGGGGCGGGGGGGGGGGGGGCGCGCGCCAGGCGGGGCGGGGCGGGGCGAGGGGCGGGGCGGGGCGAGGCG GAGAGGTGCGGCGGCAGCCAATCAGAGCGGCGCGCTCCGAAAGTTTCCTTTTATGGCGAGGCGGCGGCGGCGGCGGCCCTATAAAAAGCGAAGCGCGCGGCGGGCGGGAGTCGAGT CGCTGCGTTGCCTTCGCCCCGTGCCCCGCTCCGCCGCCGCCTCGCGCCGCCCGCCCCGGCTCTGACTGACCGCGTTACTCCCACAGGTGAGCGGGCGGGACGGCCCTTCTCCTCCG GGCTGTAATTAGCGCTTGGTTTAATGACGGCTTGTTTCTTTTCTGTGGCTGCGTGAAAGCCTTGAGGGGCTCCGGGAGGGCCCTTTGTGCGGGGGGAGCGGCTCGGGGGGTGCGTGCG TGTGTGTGTGCGTGGGGAGCGCCGCGTGCGGCTCCGCGCTGCCCGGCGGCTGTGAGCGCTGCGGGCGCGGCGCGGGGCTTTGTGCGCTCCGCAGTGTGCGCGAGGGGAGCGCGGC CGGGGGCGGTGCCCCGCGGTGCGGGGGGGGCTGCGAGGGGAACAAAGGCTGCGGGCGGGGTGTGTGCGTGGGGGGGTGAGCAGGGGGTGTGGGCGCGTCGGTCGGGCTGCAAC CCCCCCTGCACCCCCCTCCCCGAGTTGCTGAGCACGGCCCGGCTTCGGGTGCGGGGCTCCGTACGGGGCGTGGCGCGGGGCTCGCCGTGCCGGGCGGGGGGTGGCGGCAGGTGG GGGTGCCGGGCGGGGCGGGGCCGCCTCGGGCCGGGGAGGGCTCGGGGGAGGGGCGCGGCGGCCCCCGGAGCGCCGGCGGCTGTCGAGGCGCGGCGAGCCGCAGCCATTGCCTT TTATGGTAATCGTGCGAGAGGGCGCAGGGACTTCCTTTGTCCCAAATCTGTGCGGAGCCGAAATCTGGGAGGCGCCGCCGCACCCCCTCTAGCGGGCGCGGGGCGAAGCGGTGCGGC GCCGGCAGGAAGGAAATGGGCGGGGAGGGCCTTCGTGCGTCGCCGCGCCGCCGTCCCCTTCTCCCTCTCCAGCCTCGGGGCTGTCCGCGGGGGGACGGCTGCCTTCGGGGGGGAC GGGGCAGGGCGGGGTTCGGCTTCTGGCGTGTGACCGGCGGCTCTAGAGCCTCTGCTAACCATGTTCATGCCTTCTTCTTTTTCCTACAG
mPGK	CTACCGGGTAGGGGAGGCGCTTTTCCCAAGGCAGTCTGGAGCATGCGCTTTAGCAGCCCCGCTGGGCACTTGGCGCTACACAAGTGGCCTCTGGCCTCGCACACATTCCACATCCACC GGTAGGCGCCAACCGGCTCCGTTCTTTGGTGGCCCCTTCGCGCCACCTTCTACTCCTCCCCTAGTCAGGAAGTTCCCCCCCGCCCCGCAGCTCGCGTCGTGCAGGACGTGACAAATGG AAGTAGCACGTCTCACTAGTCTCGTGCAGATGGACAGCACCGCTGAGCAATGGAAGCGGGTAGGCCTTTGGGGCAGCGGCCAATAGCAGCTTTGCTCCTTCGCTTTCTGGGCTCAGAGG CTGGGAAGGGGTGGGTCCGGGGGCGGGCTCAGGGGCGGGCTCAGGGGCGGGGCGGGCGCCCGAAGGTCCTCCGGAGGCCCGGCATTCTGCACGCTTCAAAAGCGCACGTCTGCCG CGCTGTTCTCCTCTTCCTCATCTCCGGGCCTTTCGACCTGCATCC
hUbC	GATCTGGCCTCCGCGCCGGGTTTTGGCGCCTCCCGCGGGCGCCCCCCTCCTCACGGCGAGCGCTGCCACGTCAGACGAAGGGCGCAGCGAGCGTCCTGATCCTTCCGCCCGGACGC TCAGGACAGCGGCCCGCTGCTCATAAGACTCGGCCTTAGAACCCCAGTATCAGCAGAAGGACATTTTAGGACGGGACTTGGGTGACTCTAGGGCACTGGTTTTCTTTCCAGAGAGCGGA ACAGGCGAGGAAAAGTAGTCCCTTCTCGGCGATTCTGCGGAGGGATCTCCGTGGGGCGGTGAACGCCGATGATTATATAAGGACGCGCCGGGTGTGGCACAGCTAGTTCCGTCGCAGC CGGGATTTGGGTCGCGGTTCTTGTTTGTGGATCGCTGTGATCGTCACTTGGTGAGTAGCGGGCTGCTGGGCTGGCCGGGGCTTTCGTGGCCGCCGGGCCGCTCGGTGGGACGGAAGC GTGTGGAGAGAGGCCGCCAAGGGCTGTAGTCTGGGTCCGCGAGCAAGGTTGCCCTGAACTGGGGGTTGGGGGGAGCGCAGCAAAATGGCGGCTGTTCCCGAGTCTTGAATGGAAGAG GCTTGTGAGGCGGGCTGTGAGGTCGTTGAAACAAGGTGGGGGGCATGGTGGGCGGCAAGAACCCAAGGTCTTGAGGCCTTCGCTAATGCGGGAAAGCTCTTATTCGGGTGAGATGGG CTGGGGCACCATCTGGGGACCCTGACGTGAAGTTTGTCACTGACTGGAGAACTCGGTTTGTCGTCTGTTGCGGGGGCGGCAGTTATGGCGGTGCCGTTGGGCAGTGCACCCGTACCTT TGGGAGCGCGCGCCCTCGTCGTGTCGTGACGTCACCCGTTCTGTTGGCTTATAATGCAGGGTGGGGCCACCTGCCGGTAGGTGTGCGGTAGGCTTTTCTCCGTCGCAGGACGCAGGGT TCGGGCCTAGGGTAGGCTCTCCTGAATCGACAGGCGCCGGACCTCTGGTGAGGGGAGGGATAAGTGAGGCGTCAGTTTCTTTGGTCGGTTTTATGTACCTATCTTCTTAAGTAGCTGAA GCTCCGGTTTTGAACTATGCGCTCGGGGTTGGCGAGTGTGTTTTGTGAAGTTTTTTAGGCACCTTTTGAAATGTAATCATTTGGGTCAATATGTAATTTTCAGTGTTAGACTAGTAAATTGTC CGCTAAATTCTGGCCGTTTTTGGCTTTTTTGTTAG

Table 2: DNA sequences

Name	Sequence
Promoter region (hEF1a) FW	AACGTATGTCGAGGTAGGCG
Promoter region (hEF1a) RV	CAACTTCTCGGGGACTGTGG
IGF2 FW	CTGTGGCCTGTAGGTCCTTG
IGF2 RV	CCTCTGCCTTTCCCTCTTGG
TSH2B	Diagenode Cat. No. C17011041
gRNA AAVS1	CACCCCACAGTGGGGCCACT

Table 3: Primer and gRNA sequences (5'-3')

3 Supplementary Figures

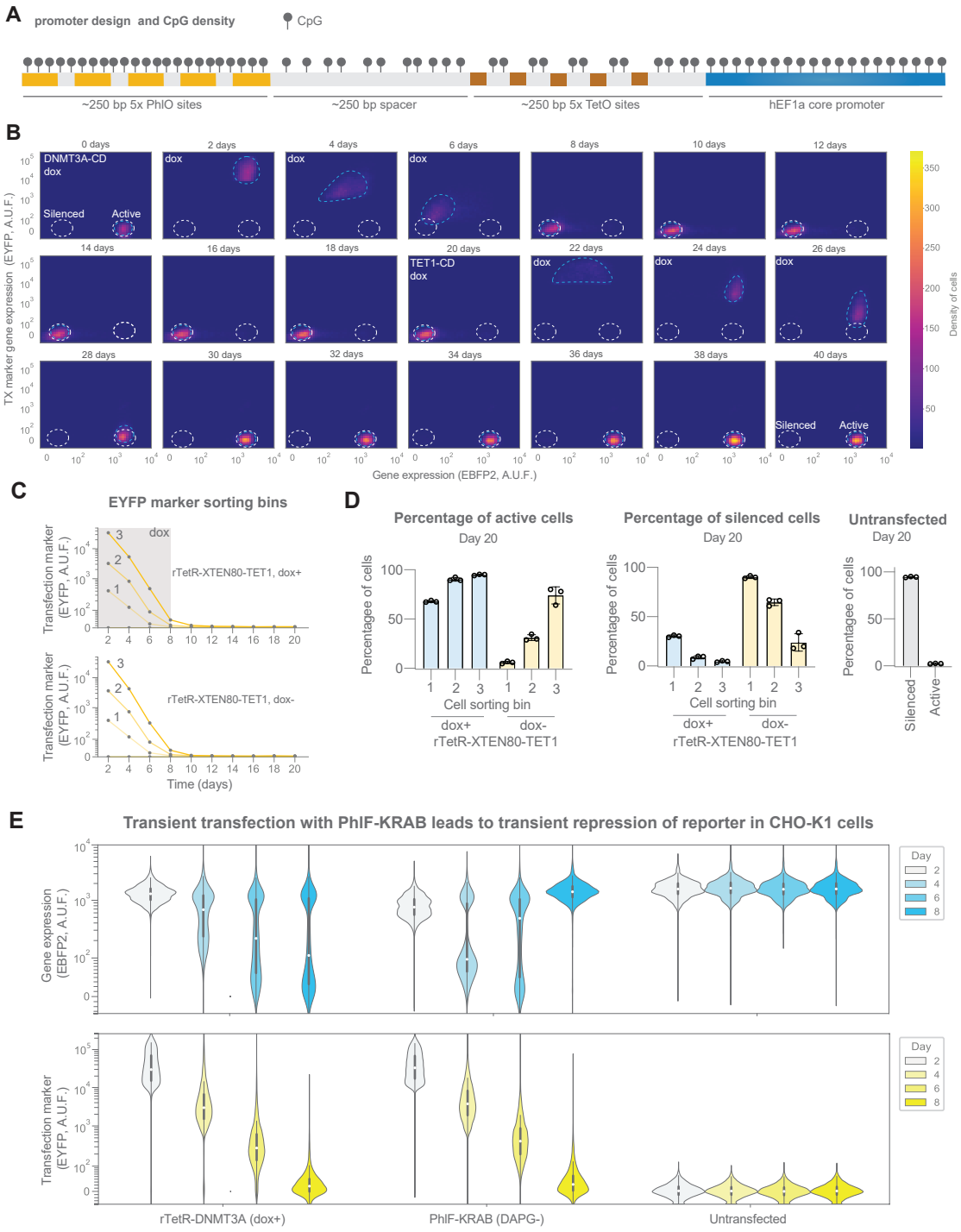

Fig. S1. Chromatin regulation in CHO-K1 cells. A. Design of operator-promoter pair used to drive reporter gene expression and distribution of CpG sites. Not to scale. The hEF1a promoter intron is not shown. This panel is related to Fig. 1A. **B.** Density scatter plot of the time course flow cytometry for repression and reactivation of CHO-K1 cells by transient transfection. This panel is related to Fig. 1C. **C.** EYFP expression levels for three different sorting bins (1-3) after rTetR-TET1 transfection with or without doxycyline (dox+/-). **D.** Bar plots showing the percentage percentages of active and silenced cells at day 20 after transfection with rTetR-TET1 (dox+/-) for the different bins sorted. **E.** Violin plots showing reporter gene expression (EBFP2) and transfection marker expression (EYFP) with rTetR-DNMT3A or PhlF-KRAB over 8 days. Data are plotted from three independent replicates. The white dot represents the median, the thick box represents the interquartile range (IQR) and the thin gray line represents 1.5x the IQR.

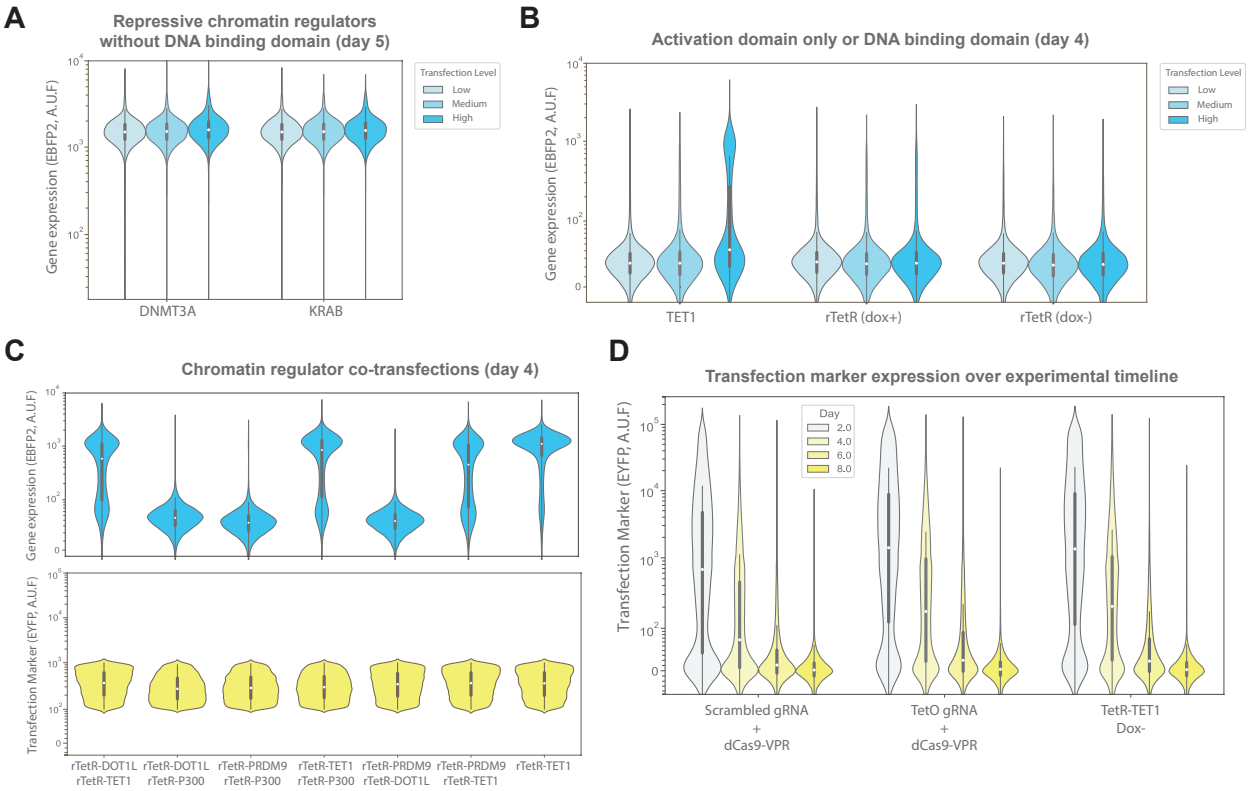

Fig. S2. Non-targeting chromatin regulators and transfection marker levels. A. Violin plots showing transfection of repressive chromatin regulators without DNA binding domain. **B.** Violin plots showing transfection of activation domain (TET1) without DNA binding domain, or DNA binding domain only (rTetR) in presence or absence of doxycycline (dox). **C.** Violin plots showing reporter gene expression and transfection marker expression for transient co-transfection of various activating chromatin regulators. This panel is related to Fig. 1E. **D.** Violin plots of transfection marker expression for dCas9-VPR and TetR-TET1 modulation comparison. This panel is related to Fig. 1F. For all violin plots, data are plotted from three independent replicates. The white dot represents the median, the thick box represents the interquartile range (IQR) and the thin gray line represents 1.5x the IQR.

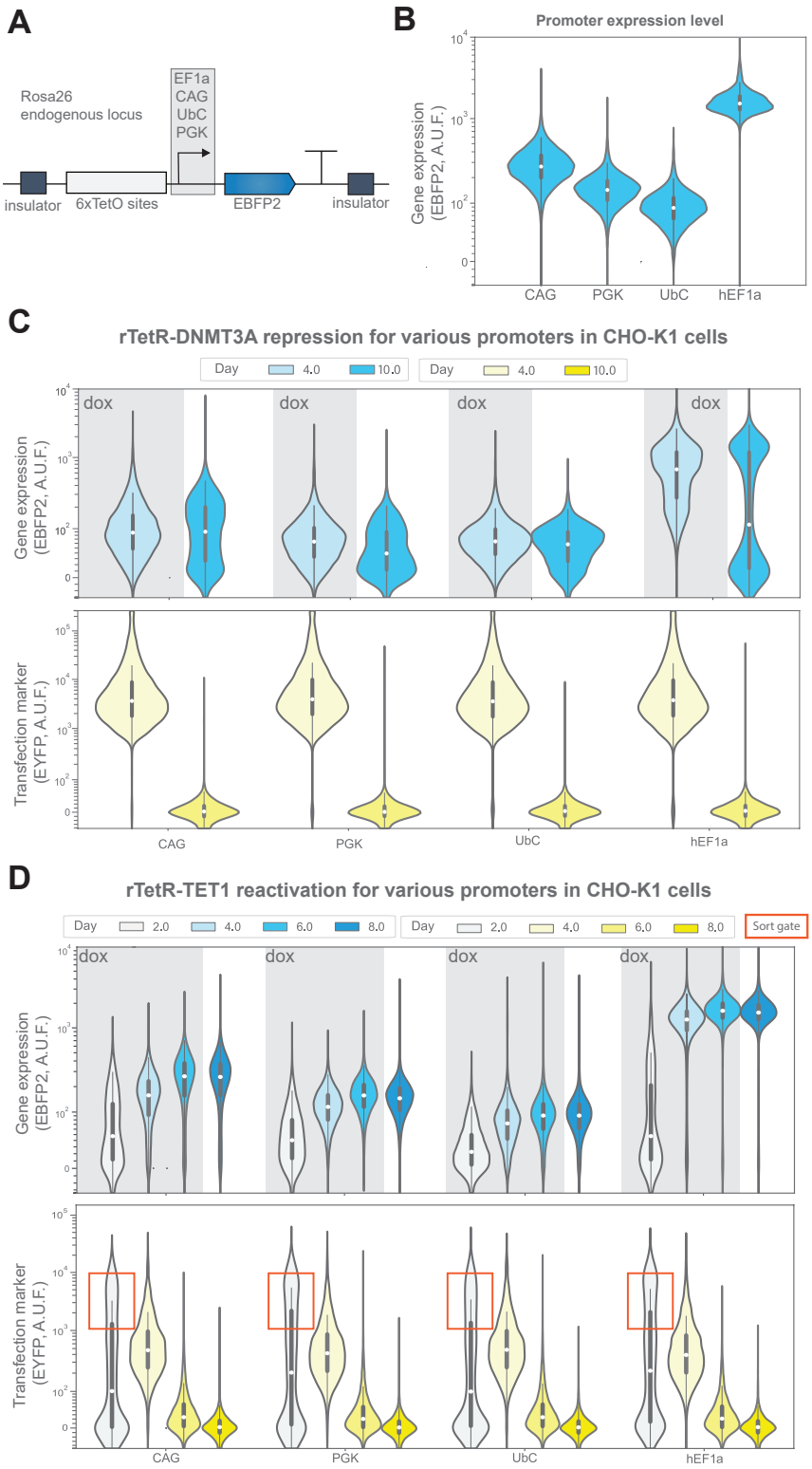

Fig. S3. Comparison of mammalian constitutive promoters for silencing and reactivation dynamics in CHO-K1 cells. **A.** Schematic showing reporter construct with the various constitutive promoters employed (CAG, mPGK, hUbC and hEF1a). **B.** Violin plots comparing promoter output of EBFP2 fluorescence following site-specific integration. **C.** Violin plots comparing silencing dynamics of the various promoters following transient rTetR-DNMT3A transfection. **D.** Violin plots comparing reactivation dynamics of the various promoters following transient rTetR-TET1 transfection. For all violin plots, data are plotted from three independent replicates. The white dot represents the median, the thick box represents the interquartile range (IQR) and the thin gray line represents 1.5x the IQR.

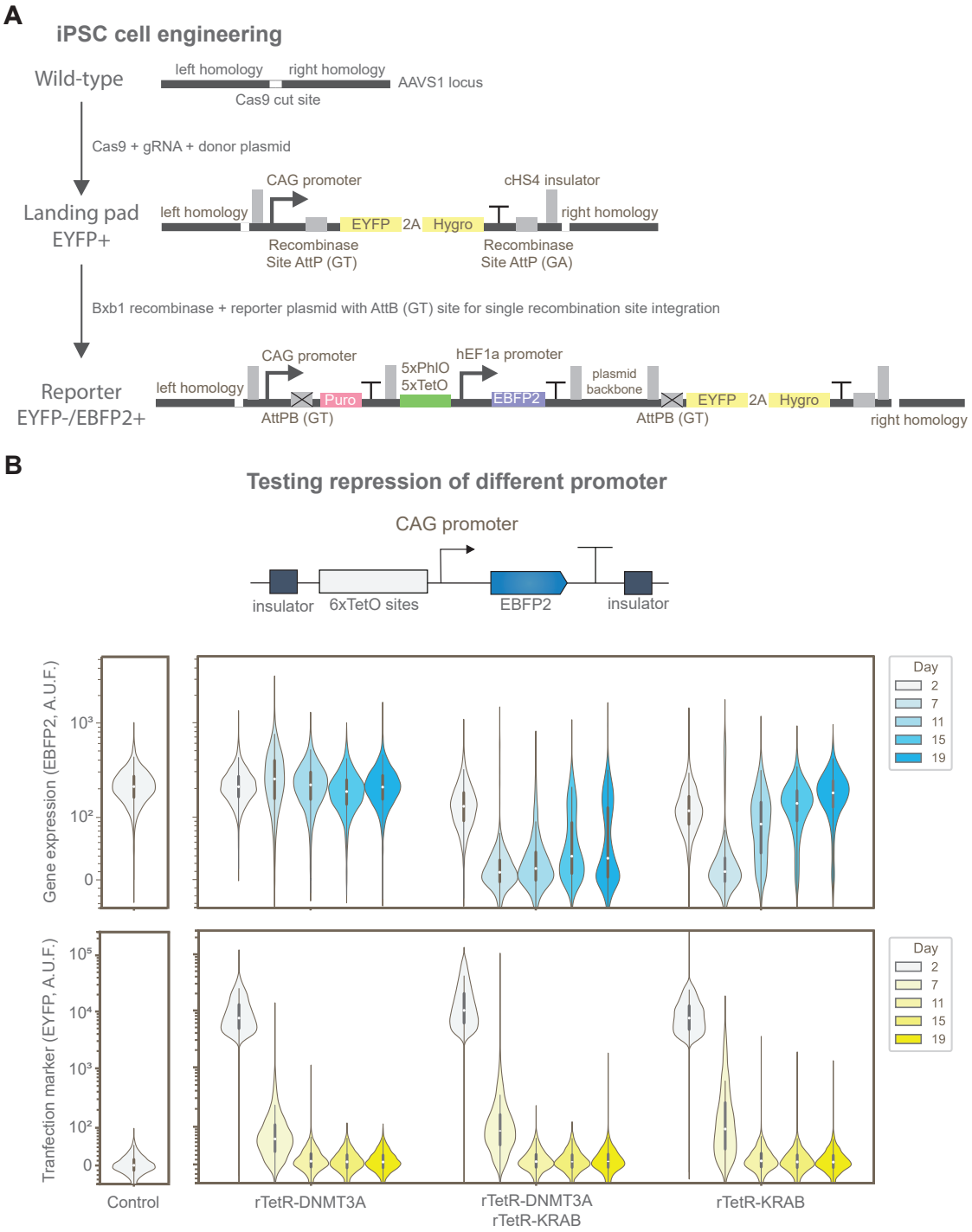

Fig. S4. iPSC engineering and testing silencing dynamics of CAG promoter. A. Schematic showing design generation of landing pad cell line followed by the reporter line. This panel is related to Fig. 2A. See Methods for details regarding integration. **B.** Violin plots showing silencing dynamics of the CAG promoter following transient transfection of rTetR-DNMT3a, rTetR-KRAB or both. Data are plotted from two independent replicates. The white dot represents the median, the thick box represents the interquartile range (IQR) and the thin gray line represents 1.5x the IQR.

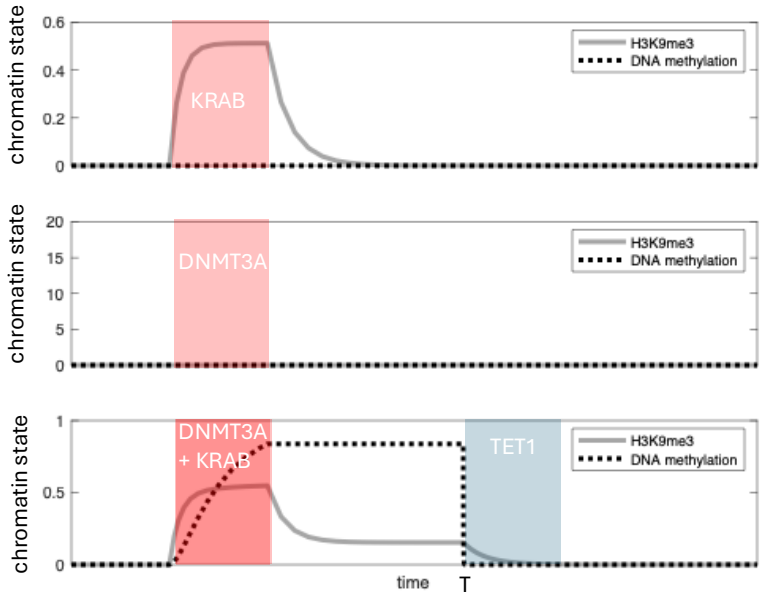

Fig. S5. Simulation results when writing DNA methylation requires H3K9me3 to be present. Simulation results from the ODE model in SI Section 1, in which $\alpha = 0.1$, $\delta = 1$, $\beta = \beta_0 = 0.1$, $T = 10$, $K = \{0, 1\}$, $D = \{0, 4\}$, and we have replaced $D \cdot u$ by zero, modeling that DNMT3A cannot write DNA methylation on nucleosomes devoid of H3K9me3, and we have replaced β by $\beta \cdot D$, modeling that H3K9me3 can recruit DNA methylation only when we overexpress rTetR-DNMT3A.

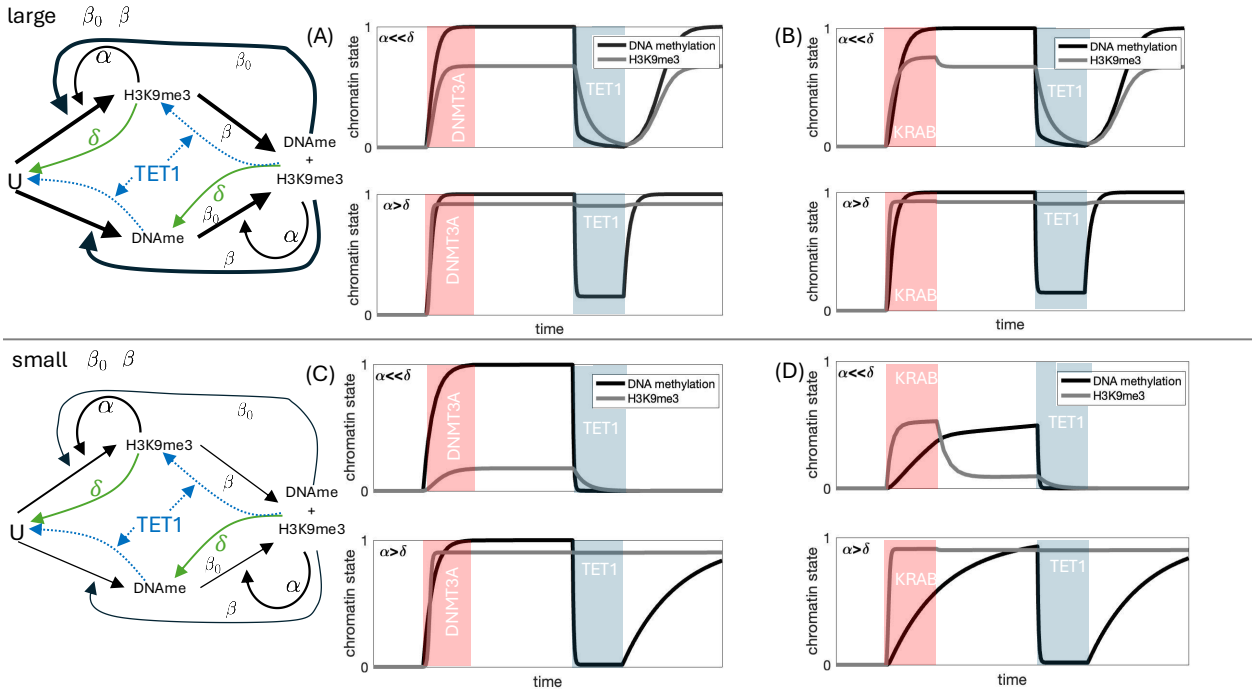

Fig. S6. Effect of the strength of the positive feedback between DNA methylation and H3K9me3 on the ability of TET1 to permanently remove H3K9me3. A-B. When the positive feedback between DNA methylation and H3K9me3 is sufficiently strong (β and β_0 are large), independent of whether the autocatalysis of H3K9me3 is strong ($\alpha > \delta$), after TET1 is removed, both marks reinforce each other and build back up. **C-D.** When the positive feedback between DNA methylation and H3K9me3 is sufficiently weak (β and β_0 are large), DNA methylation and H3K9me3 will not build back up unless the autocatalysis of H3K9me3 is sufficiently strong ($\alpha > \delta$). Top: $\beta = \beta_0 = 1$. Bottom: $\beta = \beta_0 = 0.1$. Other parameter values: $\alpha = \{0.1, 10\}$, $\delta = 1$, $T = 10$, $D = 1$, and $K = 1$.

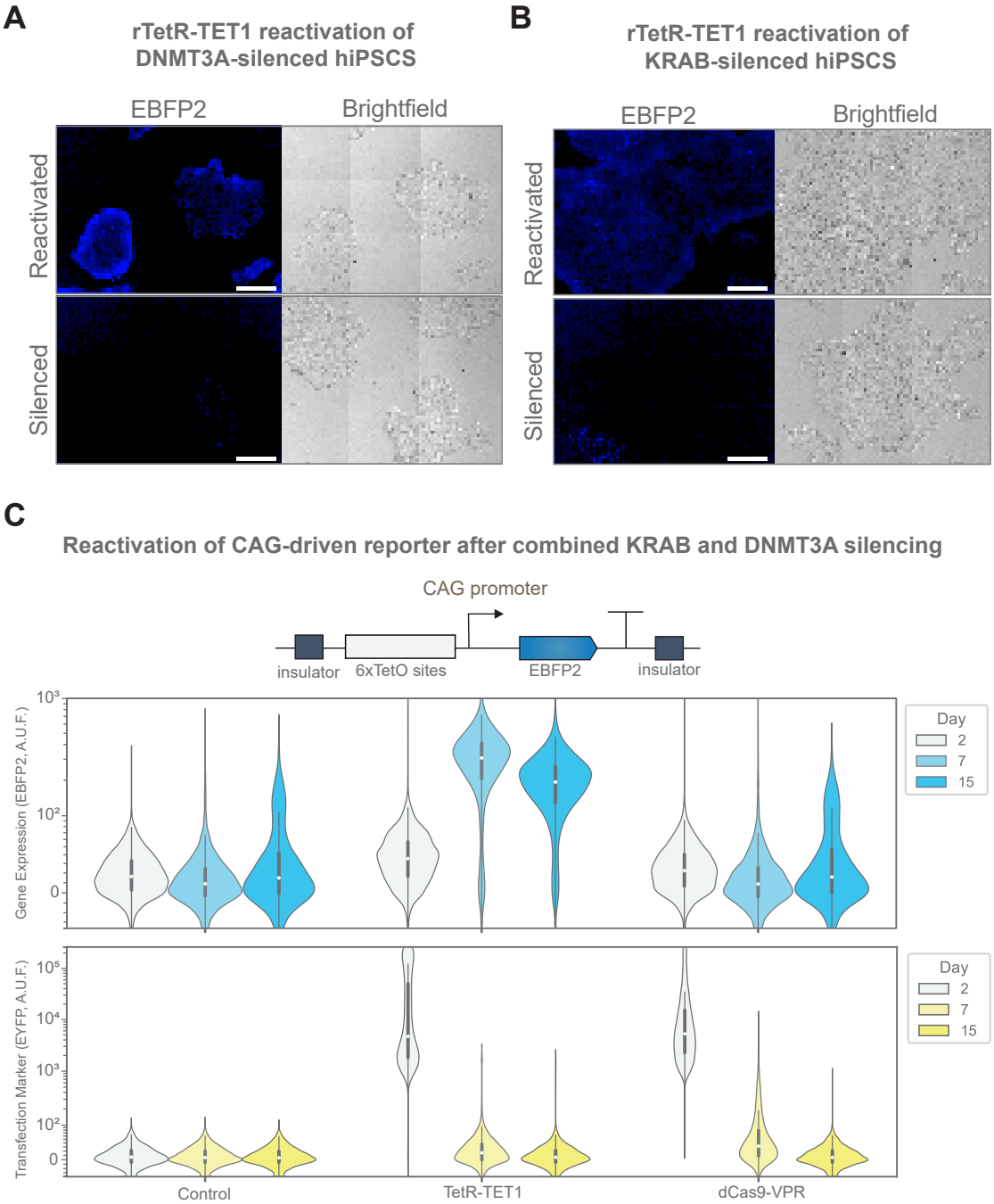

Fig. S7. Single channel microscopy images and CAG promoter reactivation. A-B. Single channels for microscopy images of rTetR-TET1 reactivation experiment following **(A)** rTetR-DNMT3A silencing or **(B)** PhlF-KRAB silencing. This panel is related to Fig. 4E and 4G. **C.** Violin plots showing TetR-TET1 mediated reactivation dynamics of CAG-driven transgene reporter in hiPSCs following silencing PhlF-KRAB and rTetR-DNMT3A co-transfections. Data are plotted from three independent replicates. The white dot represents the median, the thick box represents the interquartile range (IQR) and the thin gray line represents 1.5x the IQR.

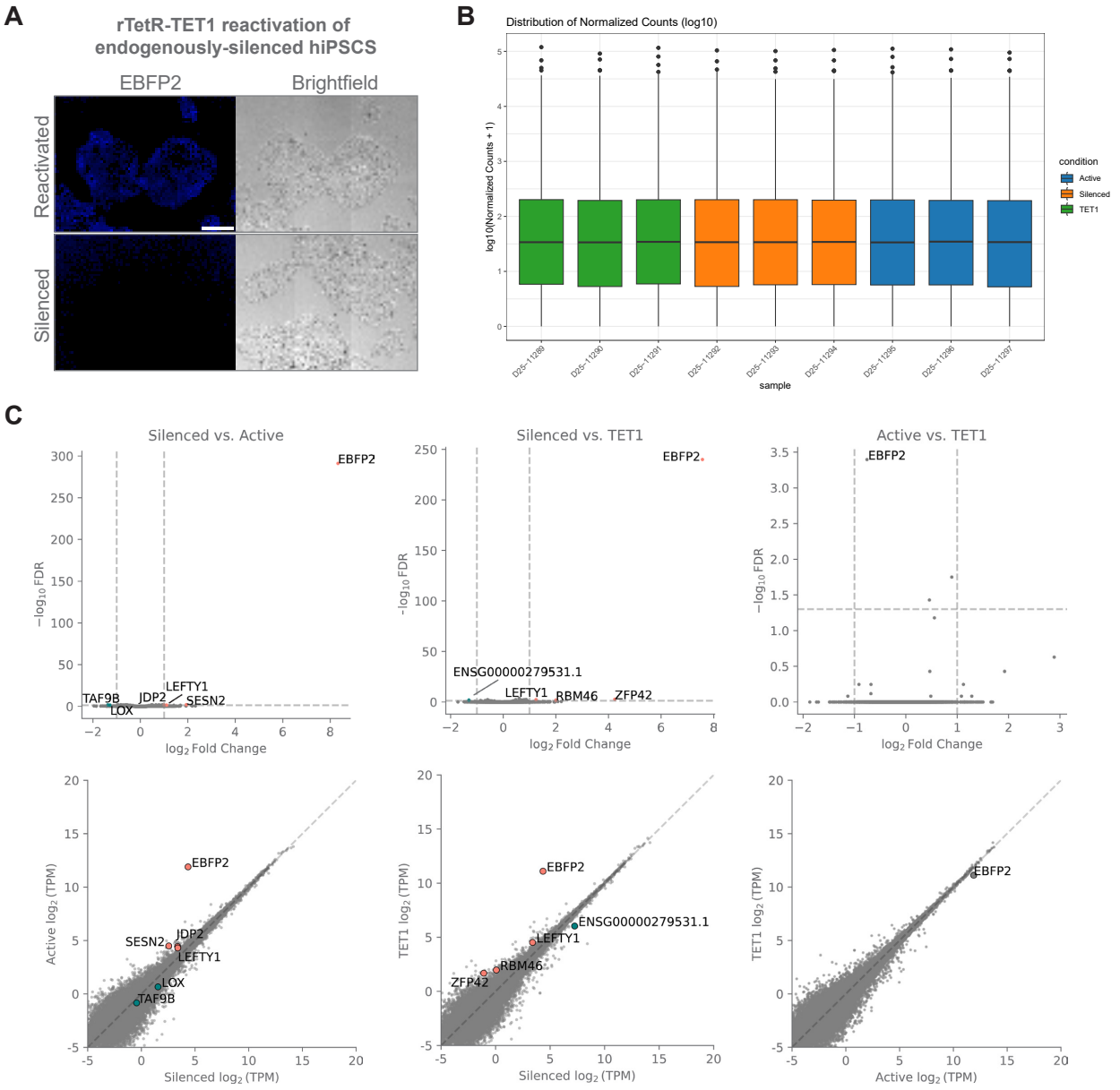

Fig. S8. Single channel microscopy images and RNA seq data. A. Single channels for microscopy images of rTetR-TET1 reactivation experiment following endogenous silencing. This panel is related to Fig. 5E. **B.** Normalized transcript counts for each replicate in RNA seq experiment. This panel are related to Fig. 5G and the following panels. **C.** Volcano plots and transcript counts of RNA seq data for the different conditions. These panels are related to Fig. 5G. TPM: Transcripts per million; FDR: False discovery rate.

4 Supplementary Methods

Cell culture, seeding, transfection, sorting and flow analysis were performed as described in Main Methods. The following methods describe the amounts of DNA transfected for each experiment appearing in the Supplementary Figures.

Comparing DNMT3A and KRAB silencing in CHO-K1 cells (S1E). 500 ng of rTetR-DNMT3A or PhlF-KRAB was transfected with 300 ng EYFP marker with Lipfectamine LTX to 150,000 cells in a 12 well plate seeded the day before. Sorting was performed on day 2, and flow cytometry measurements were acquired after sorting and every other day thereafter until day 8.

Non-targeted chromatin regulators (S2A). 500 ng of DNMT3A or KRAB without fusion to DNA binding domain was transfected along with 300 ng EYFP as described in Methods. On day 5 after transfection, cells were analyzed by flow cytometry. The data were computationally binned for EYFP marker expression and plotted accordingly.

TET1 or rTetR for reactivation (S2B). 500 ng of TET1 without a DNA binding domain or 500 ng of rTetR without a catalytic domain were transfected along with 300 ng EYFP marker. On day 4 after transfection, cells were analyzed by flow cytometry. The data were computationally binned for EYFP marker expression and plotted accordingly. For rTetR transfections, 2 µM doxycycline was used throughout the experiment.

Silencing and reactivation of various promoters in CHO-K1 cells (S3C-D). For silencing, 500 ng rTetR-DNMT3A and 300 ng EYFP were transfected. Doxycycline was administered for 8 days. For reactivation, 500 ng rTetR-TET1 and 300 ng EYFP were used. Dox was administered for 6 days. The final dox concentration was 2 µM.

Silencing of CAG promoter reporter in hiPSCs (S4B). For single transfection, either 500 ng of rTetr-DNMT3A or 500 ng rTetR-KRAB were used along with 300 ng EYFP marker. For co-transfection of both chromatin regulators, 250 ng of each was transfected with 300 ng of EYFP. The cells were sorted 2 days later and monitored for 19 days. Dox (2 µM) was supplemented for 8 days after transfection.

Reactivation of silenced CAG reporter in hiPSCs (S7C). To obtain the repressed starting population, cells in the silenced state from the previous rTetR-DNMT3A and rTetR-KRAB silencing were sorted for EBFP2- and expanded. For TET1 transfections, 500 ng of TetR-TET1 and 300 ng EYFP marker were used. For VPR transfections, 250 ng of each dCas9-VPR and gRNA targeting TetO with 300 ng EYFP were used. Cells were

sorted 2 days after transfections and cultured for 15 days. Flow cytometry analysis was performed after sorting on day 2, then day 7 and 15.